CrossMark

ORIGINAL PAPER

Evaluation of NCEP TIGGE short-range forecast for Indian summer monsoon intraseasonal oscillation

Snehlata Tirkey[1] · P. Mukhopadhyay[1]

Abstract This study focuses on the short-range prediction of Monsoon Intraseasonal Oscillations (MISOs) using the National Centers for Environmental Prediction(NCEP) Ensemble Prediction System (EPS) data from The Observing System Research and Predictability Experiment (THORPEX) Interactive Grand Global Ensemble (TIGGE) archive. The Indian Summer Monsoon Rainfall (ISMR), which plays an important role in the socio-economic growth of the country, is highly variable and is mostly governed by the MISOs. In addition to this, deterministic forecasts of ISMR are not very reliable. Hence, a probabilistic approach at daily scale is required. Keeping this in mind, the present analysis is done by using daily forecast data for up to 7-day lead time and compared with observations. The analysis shows that the ensemble forecast well captures the variability as compared to observations even up to 7 days. The spatial characteristics and the northward propagation of MISO are observed thoroughly in the EPS. The evolution of dynamical and thermodynamical parameters such as specific humidity, moist static energy, moisture divergence, and vorticity is also captured well but show deviation from the observation from 96 h lead time onwards. The tropospheric temperature forecast captures the observed gradient but with certain bias in magnitude whereas the wind shear is simulated quite well both in pattern and magnitude. These analyses bring out the biases in TIGGE EPS forecast and also point out the possible moist processes which needs to be improved.
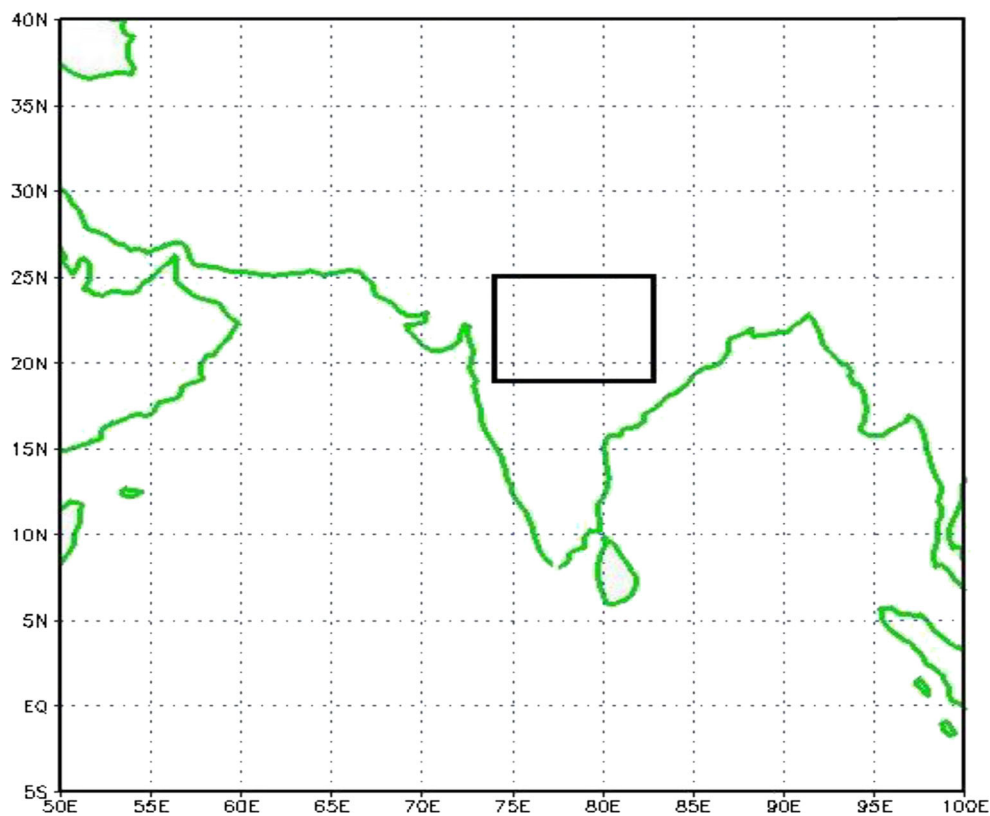
1 Introduction

The Indian Summer Monsoon is the seasonal change of winds and rainfall over the Indian region. It can be interpreted as a manifestation of northward seasonal migration of the east–west-oriented precipitation belt or cloudiness i.e. the Tropical Convergence Zone (TCZ) (Yasunari 1979; Sikka and Gadgil 1980; Gadgil 2003). The rain-bearing systems during monsoon such as low pressure systems and monsoon depressions, having timescales of 5–7 days, account significantly for the monsoon rainfall. In addition to this, the periods of dry and wet spells often spanning 2–3 weeks are also a major factor in determining it (Goswami 2005). These wet and dry spells of the ISM rainfall are affected by the northward propagating boreal summer monsoon intraseasonal oscillations (MISO). These quasi-periodic oscillations are the fluctuations of the regional Hadley circulation, which is a manifestation of the northward shift of the ITCZ over the Indian monsoon region (Yasunari 1981; Krishnamurti and Subramanyam 1982). Among the different modes of the ISOs, the active/break spells in ISM rainfall are largely determined by the northward propagating 30–60-day mode (Sikka and Gadgil 1980; Goswami 2005), and therefore the

✉ P. Mukhopadhyay
 mpartha@tropmet.res.in

[1] Indian Institute of Tropical Meteorology, Dr. Homi Bhabha Road,
 Pune 411008, India

Fig. 1 Box over Central India (18°N–25°N, 73°E–85°E) taken for the Central India precipitation index

prediction of this northward propagating low-frequency 30–60-day rainfall anomaly is of great importance as it affects the agricultural productivity and hence affects our country's economy (Gadgil and Gadgil 2006).

The prediction of the Indian Summer Monsoon Rainfall (ISMR) and its variability is one of the most challenging tasks for the modellers either by empirical or dynamical numerical models. Systematic errors in the models, inaccurate parameterization schemes and computational inefficiency are some reasons for it (Chen and Alpert 1990; Chen et al. 1992; Waliser 2012). Limited predictability of most models is due to the major systematic biases inherent in them in simulating the seasonal mean ISMR and a great deal of uncertainty in reproducing its inter-annual variability (IAV). Goswami et al. (2006) explain two distinct classes of processes that govern the IAV of monsoon rainfall as follows. Slowly evolving processes like coupled ocean–atmosphere oscillations, Tibetan Plateau heating, Eurasian snow cover changes, soil moisture changes, etc., modulate the annual monsoon cycle and are termed as external processes. The IAV arising from these slow processes or "external" forcing is less sensitive to initial condition and more predictable. On the other hand, fast or

"internal" dynamical processes occur through nonlinear interaction between the annual monsoon cycle and chaotic summer monsoon ISOs and hence probably less predictable. Therefore, the predictability of the monsoon depends on relative contributions of the external and internal components to the total IAV of the monsoon
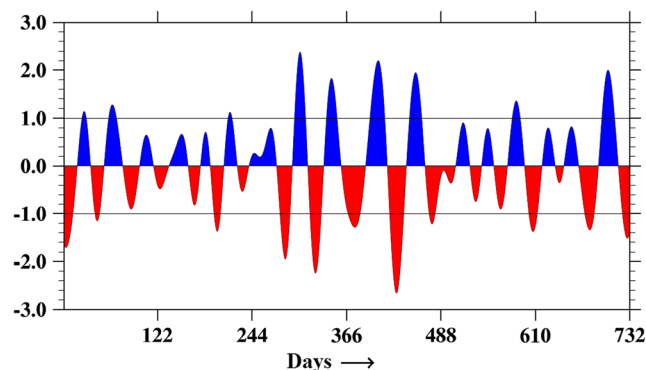
Fig. 2 Normalized filtered anomaly of rainfall (TRMM 3B42) over central India for JJAS months for the period of 2006–2011. *Red color* stands for negative and *blue* stands for positive standardized rainfall anomaly respectively

annual cycle (Goswami et al. 2006). About 50 % of the IAV is contributed by the internal component which is the ISOs. The structure and amplitude of the summer ISOs in a model depend on the hydrological cycle of the model governed, among others, by parameterization of convection and also by the land surface processes in the model (Goswami et al. 2006).

The limit of the dynamic predictability for the tropical intraseasonal oscillation was estimated by Waliser et al. (2003). They used National Aeronautics and Space Administration (NASA) Goddard Laboratory for Atmospheres (GLA) Atmospheric General Circulation Model (AGCM) to conduct a twin perturbation experiment and computed the signal to noise ratio to determine the limit. For velocity potential at 200 hPa, the limit was found to be 25 days whereas for rainfall it was 15 days. Reichler and Roads (2005) probed the predictability of the MJO and its sensitivity to initial and boundary conditions by the NCEP seasonal forecasting model at T42 resolution. They determined the limit of predictability by fixing the minimum anomaly correlation for useful skill to be 0.4 and found that the useful forecast range for velocity potential at 200 hPa came to be 4 weeks but not so for precipitation. Liess et al. (2005) used ECHAM5 atmospheric GCM to study the predictability of boreal summer ISO at T63 resolution and initialized the runs using a breeding method. They used extended EOFs and projected the forecasts on the first four EOFs. They found the upper limit of predictability over India to be 15 days for precipitation and 20 days for 200 hPa zonal
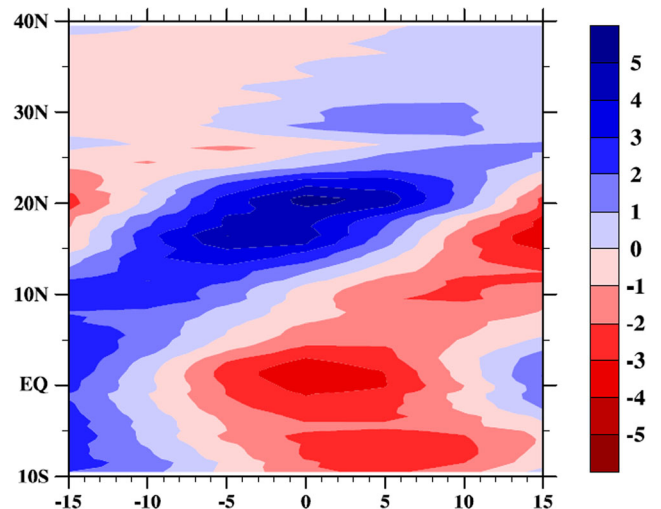

Fig. 4 Lag-latitude plot for TRMM precipitation anomaly (mm day^{-1}) averaged over 70°E–90°E for the active period

wind. These studies show that the models have some skills in predicting certain dynamical variables associated with ISO but lacks in doing so for rainfall. Also, such skill is highly dependent on the model physics as it varies from model to model.

Due to shortcomings of deterministic forecast and due to inherent chaotic nature of the nonlinearly evolving atmospheric systems (Lorenz 1963), it is preferable to embark on Ensemble Prediction System (EPS). Errors in initial conditions and model errors limit the predictability and these in turn limit the skill of the single, deterministic forecast. Ensemble prediction is a reason-
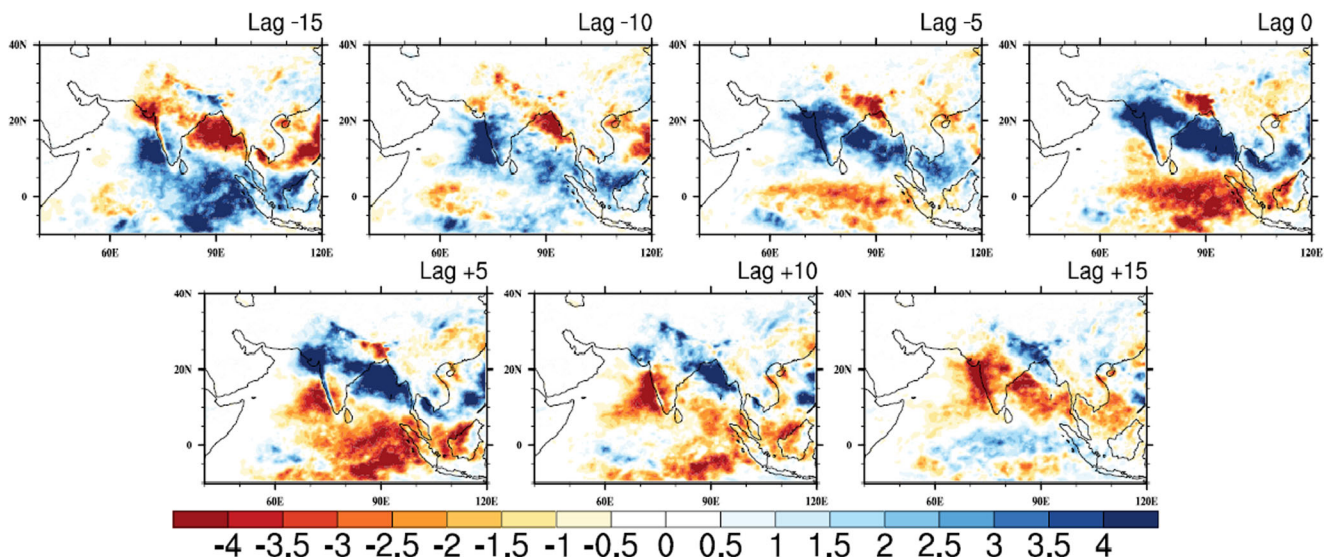

Fig. 3 Lag composite of rainfall (mm day^{-1}) during active spells based on Central India precipitation index using TRMM 3B42 data
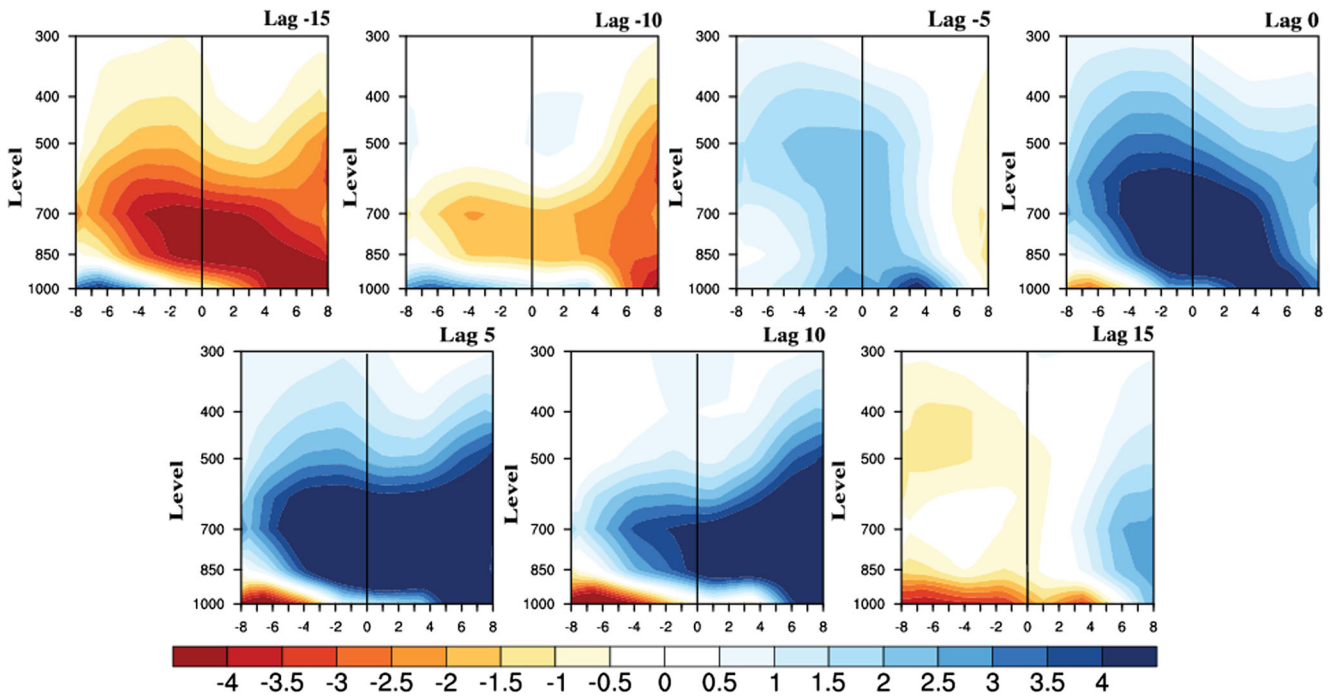
Fig. 5 Composite of meridional-vertical structure of specific humidity (kg/kg, $\times 10^{-4}$) with respect to convection centre for active period using NCEP/NCAR Reanalysis data

able way to complement a single, deterministic forecast with an estimate of the probability density function of forecast states. Such an approach may lead to a better prediction of MISO and hence in overall prediction of
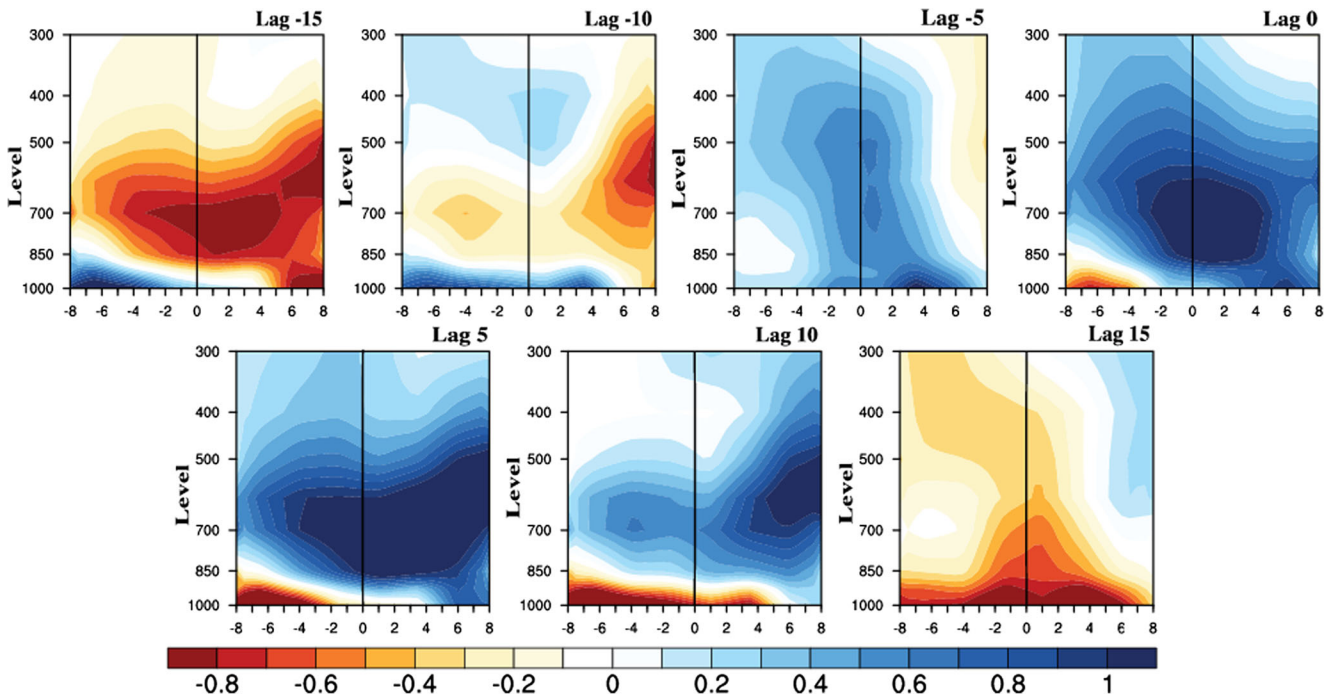

Fig. 6 Lag composite of meridional-vertical structure of moist static energy (kJ kg^{-1}) with respect to convection centre for active period using NCEP/NCAR Reanalysis data
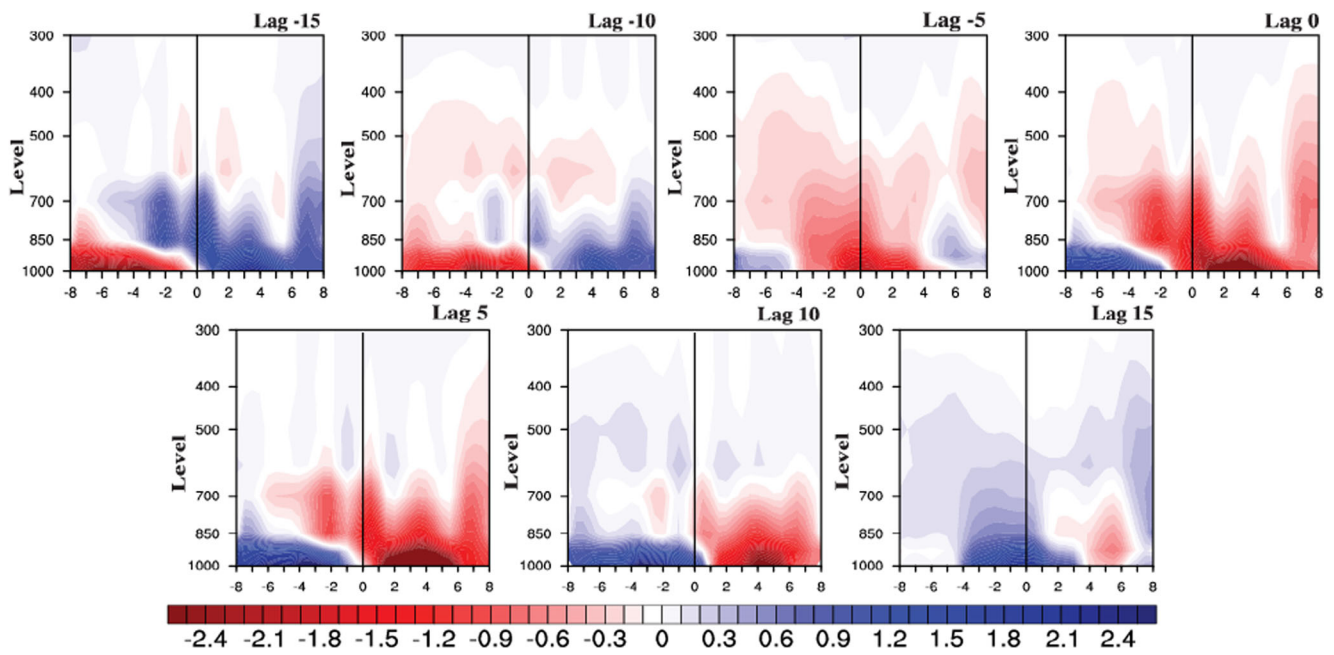
Fig. 7 Lag composite of meridional-vertical structure of moisture divergence (s^{-1}, $\times 10^{-8}$) with respect to convection centre for active period using NCEP/NCAR Reanalysis data

ISMR. Keeping this in mind, the present study is intended to evaluate the skill of TIGGE EPS for

MISO forecast. Comparison of EPS forecast data with observation would demonstrate the strength and weak-
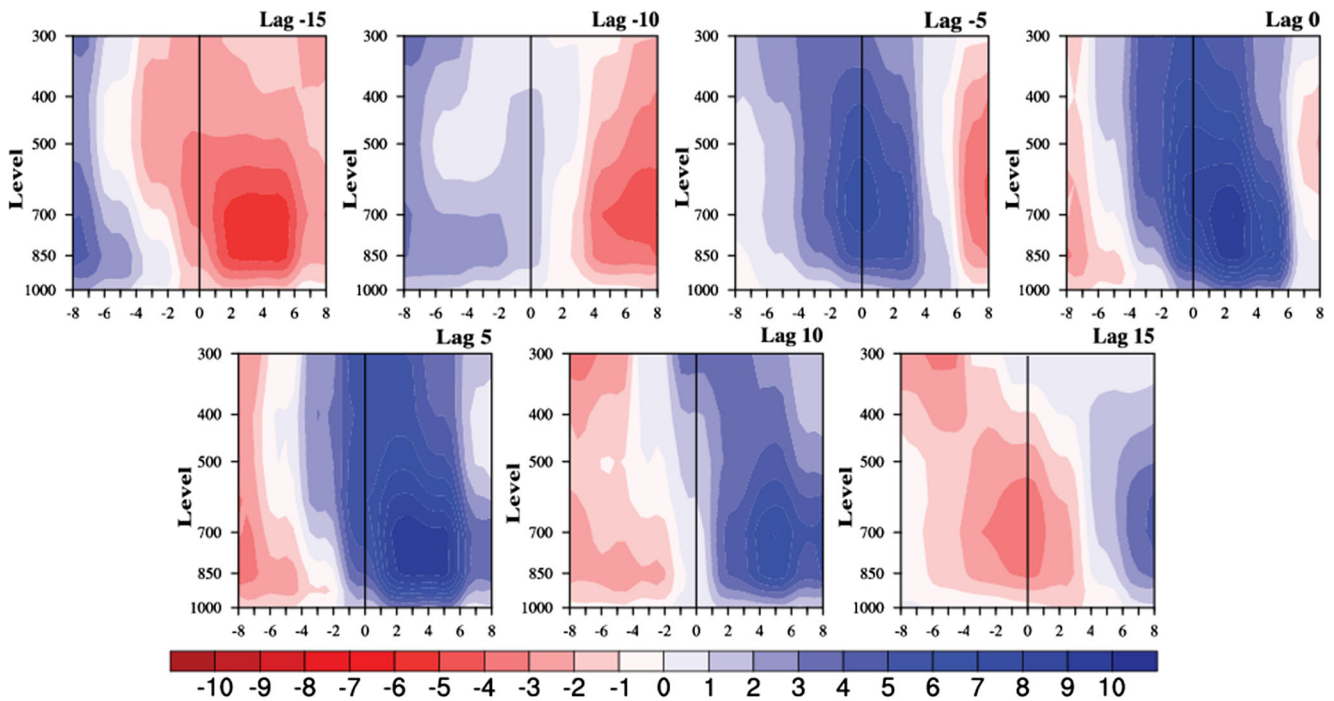

Fig. 8 Lag composite of meridional-vertical structure of vorticity (s^{-1}, $\times 10^{-6}$) with respect to convection centre for active period using NCEP/NCAR Reanalysis data

ness of EPS and also would provide necessary basis for developing much needed indigenous EPS for short-range forecast over Indian Monsoon region.

An attempt to study the EPS forecast data with respect to observation is made with parameters such as rainfall, specific humidity and temperature. We would like to see the extent to which the EPS forecast data is able to capture the observed variability and its consistency in the short range with 7-day forecast data. Analysing the daily data would give us a better insight into the short-range prediction capability of the model. The analysis of daily data to estimate the forecast fidelity of ISO with EPS will help us to observe the strengths and weaknesses of EPS. Attempt to understand the reasons behind its success or failure will also be made. This study is particularly important as the CFS/GFS ensemble-based seasonal (Yang et al. 2008; Pattanaik and Kumar 2009) and extended range forecast (Sahai et al. 2013; Abhilash et al. 2014) has already been found significantly successful in forecasting Indian summer monsoon. However, the ensemble-based short-range forecast is yet to be established.

2 Data and methodology

2.1 Observational data

The Tropical Rainfall Measuring Mission (TRMM) generated product 3B42 is used for the study (Huffman
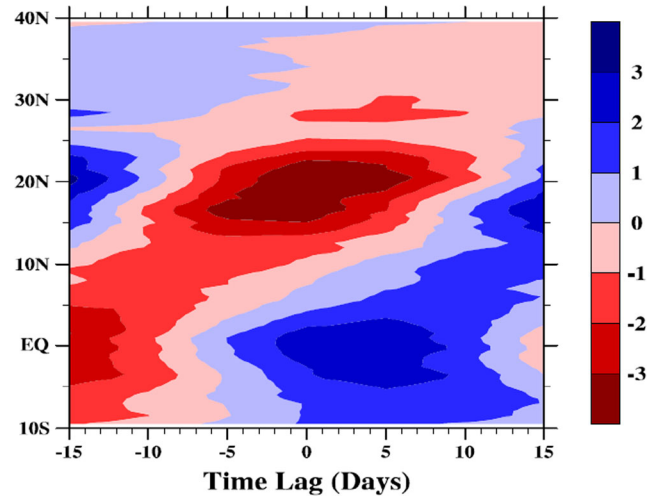

Fig. 10 Lag-Latitude plot for TRMM precipitation anomaly (mm day^{-1}) averaged over 70°E–90°E for the break period

et al. 2007). It is of 3-h temporal resolution and 0.25° by 0.25° spatial resolution. The daily accumulated (beginning at 00Z and ending at 21Z; unit, mm) rainfall product is derived from this 3-h product. The TRMM 3B42 daily data at a resolution of 0.25 × 0.25 is used for the study. The spatial coverage of the TRMM 3B42 data is from 50°S to 50°N and global longitudes. For the present study, the area under consideration is from 10°S to 40°N and 40°E to 120°E and data is taken from 2005 to 2012.
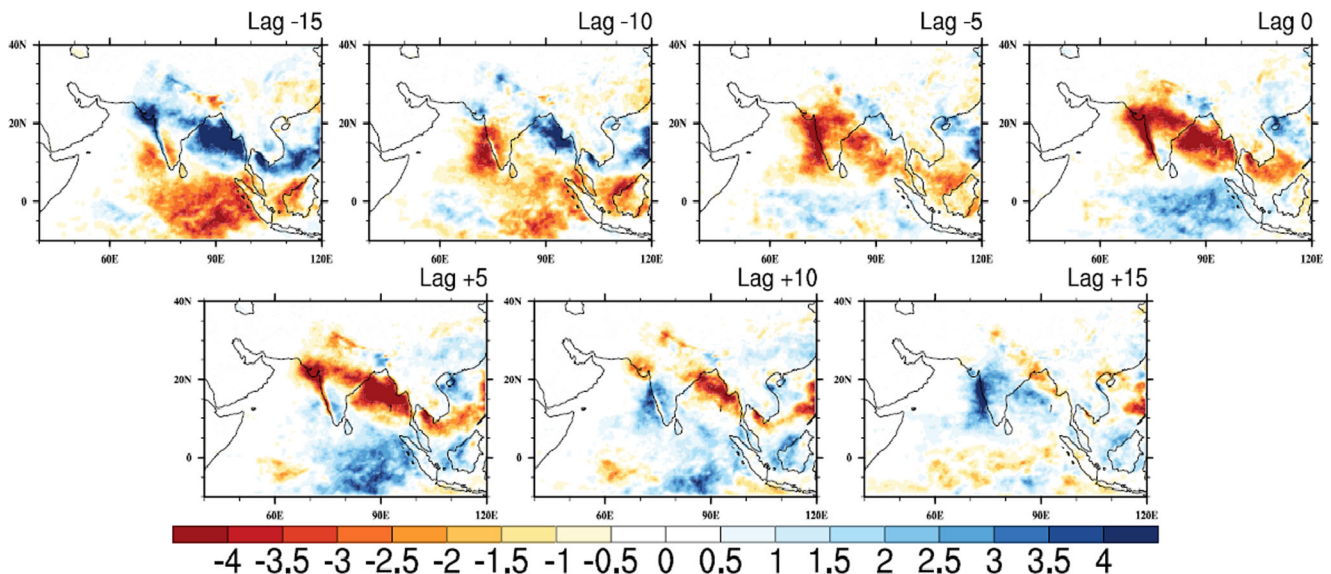

Fig. 9 Lag composite of rainfall (mm day^{-1}) during break phase based on Central India precipitation index using TRMM 3B42 data
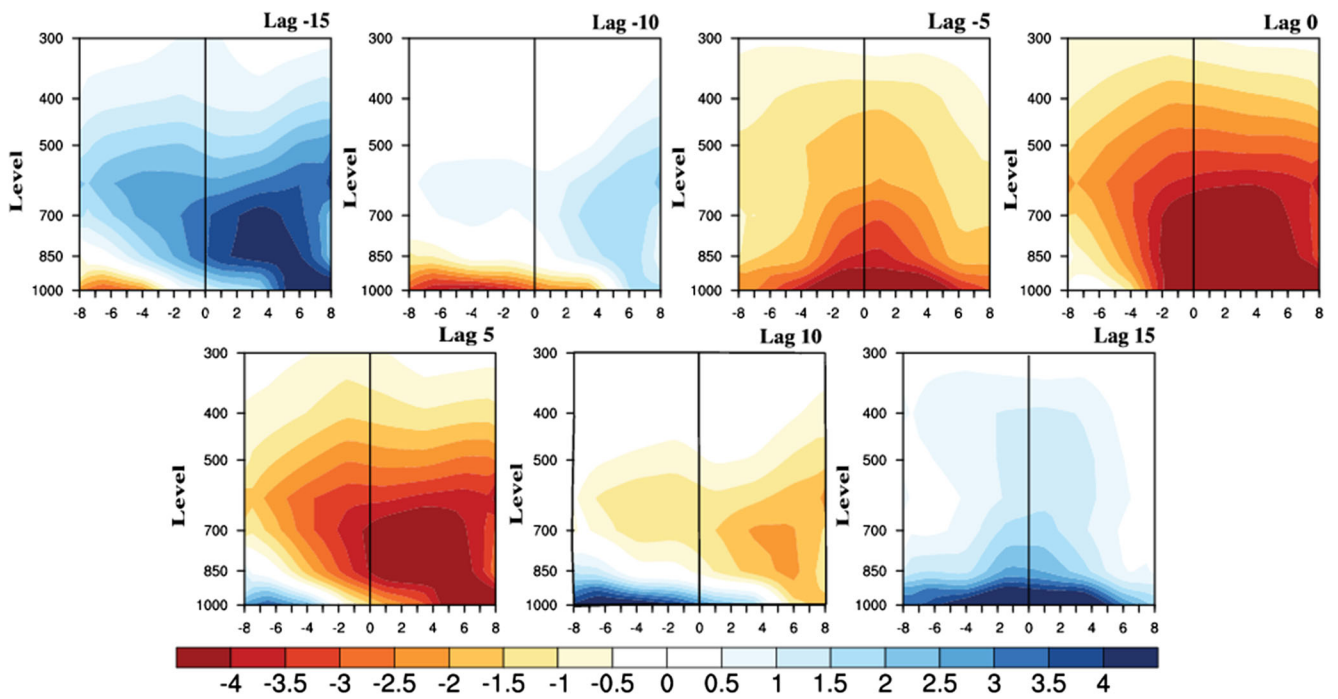
Fig. 11 Composite of meridional-vertical structure of specific humidity (kg kg^{-1}, $\times 10^{-4}$) with respect to convection centre for break period using NCEP/NCAR Reanalysis data

NCEP/NCAR reanalysis data (Kalnay et al. 1996) in 17 pressure levels and at 2.5° × 2.5° horizontal reso- lution is used for the present study. Temperature, spe- cific humidity, U component of wind, V component of
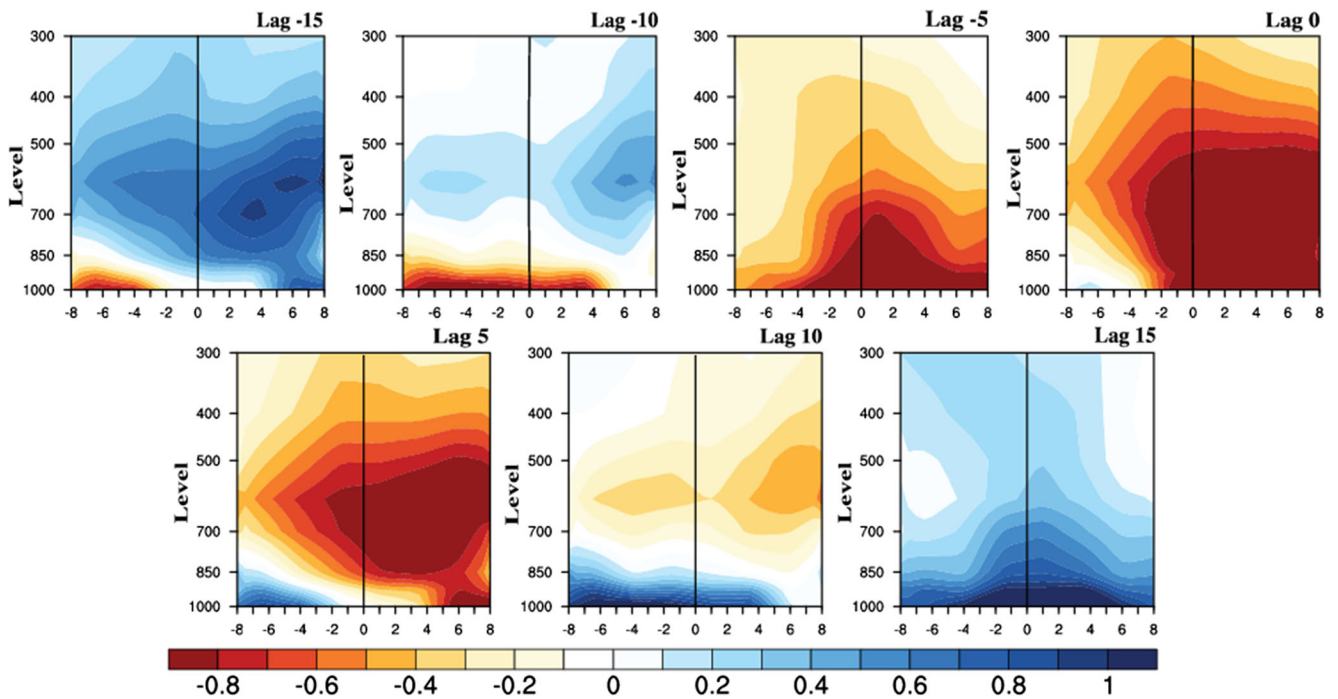

Fig. 12 Lag composite of meridional-vertical structure of moist static energy (kJ kg^{-1}) with respect to convection centre for break period using NCEP/NCAR Reanalysis data
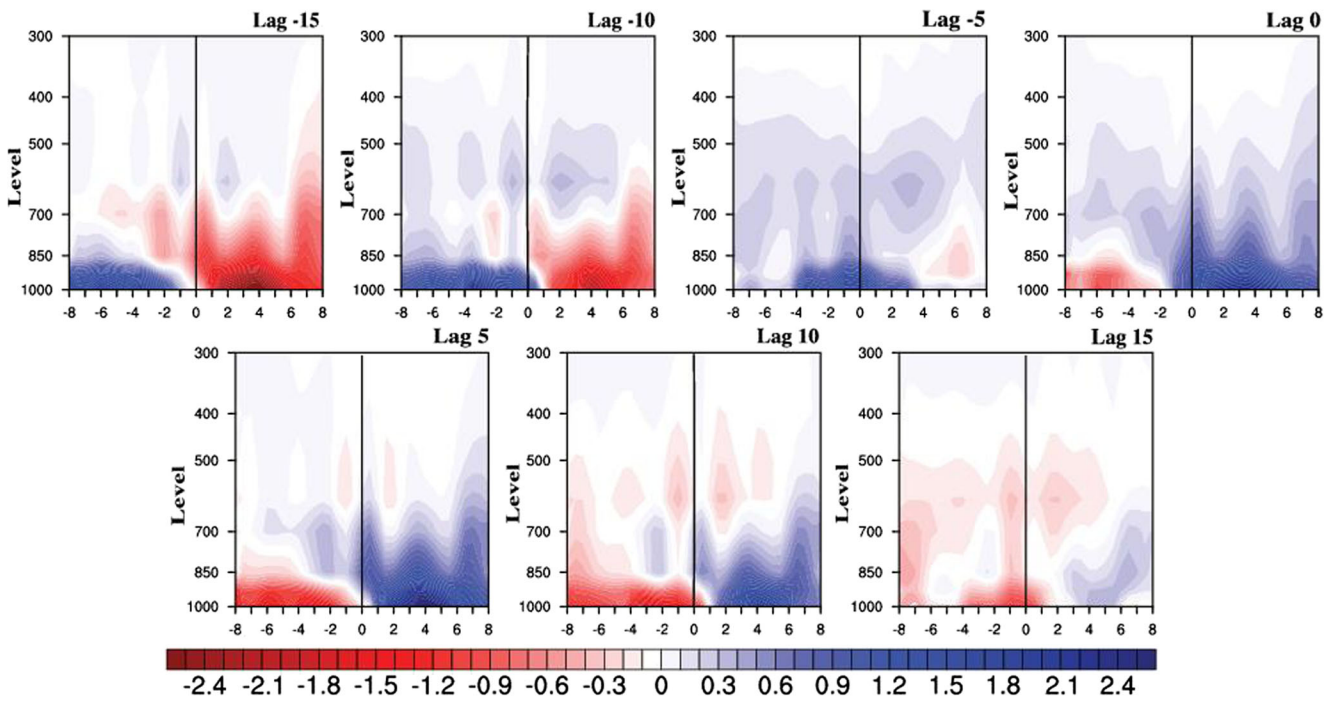
Fig. 13 Lag composite of meridional-vertical structure of moisture divergence (s^{-1}, $\times 10^{-8}$) with respect to convection centre for break period using NCEP/NCAR Reanalysis data

wind and geopotential height data, for the period 2007–2012, are used for the study. Presently, we are

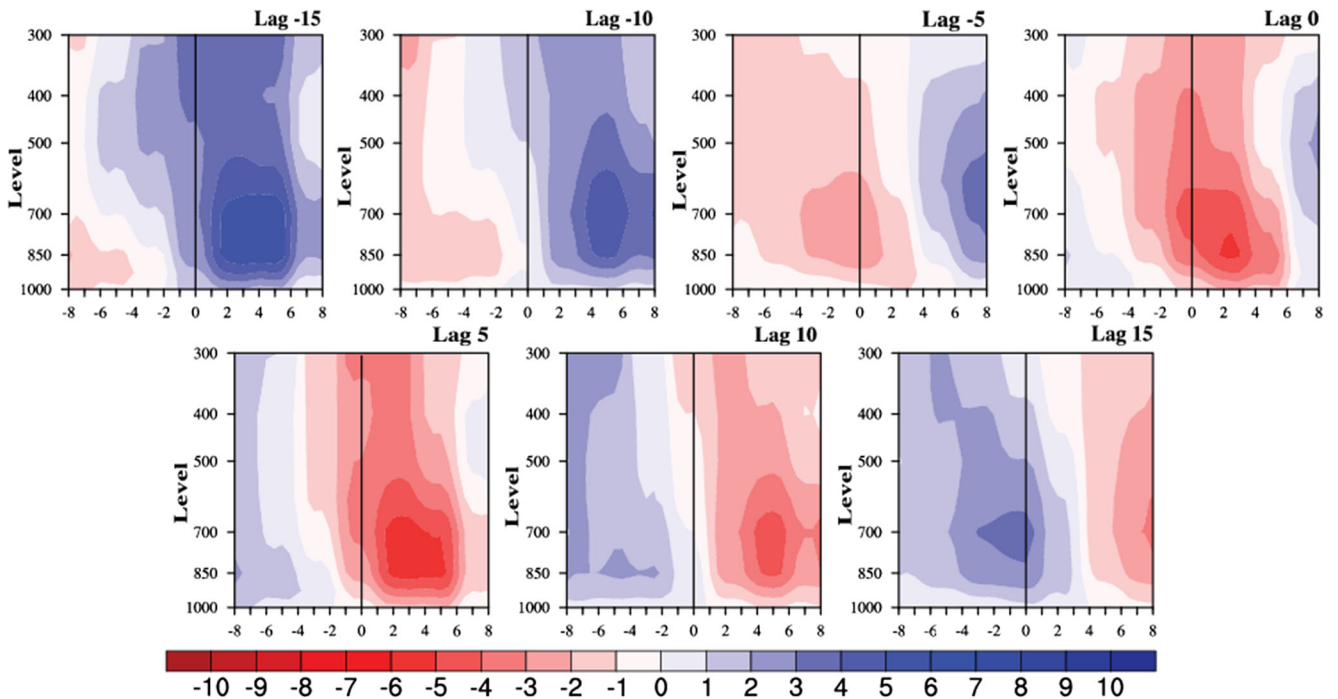using data at 1000 to 300 hPa levels for comparison with forecast. The area under consideration is 10°S–

Fig. 14 Lag composite of meridional-vertical structure of vorticity (s^{-1}, $\times 10^{-6}$) with respect to convection centre for break period using NCEP/NCAR Reanalysis data
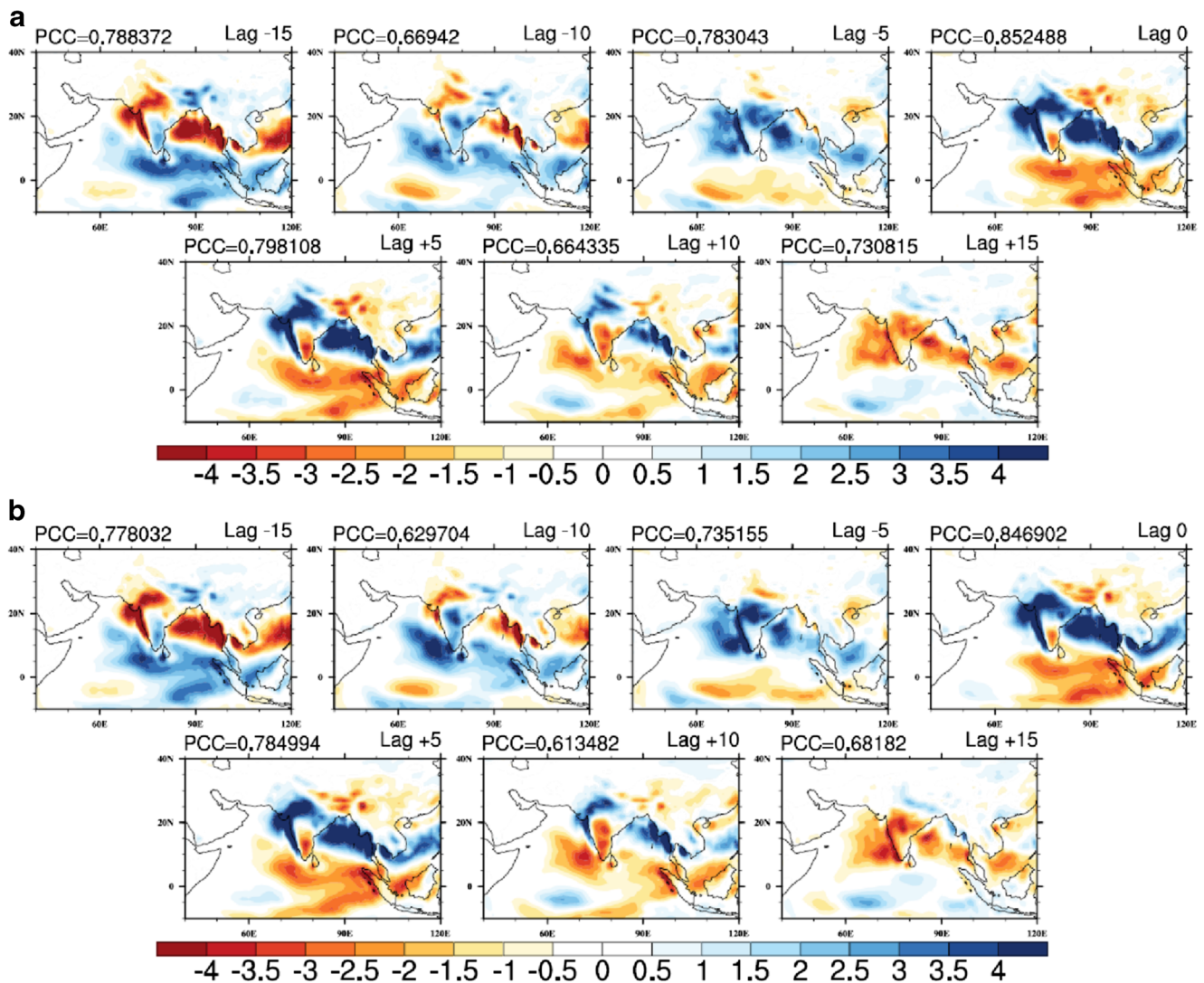
Fig. 15 Lag composite of rainfall (kg m^{-2}) during active phase from NCEP EPS data for **a** 24 h, **b** 48 h, **c** 96 h and **d** 168 h forecast lead time

40°N and 40°E–120°E. The vertical structure of specific humidity, moisture divergence, moist static energy, tropospheric temperature gradient and wind shear for both the active and break periods are computed from this data.

2.2 Forecast data

The Observing System Research and Predictability Experiment (THORPEX) is a major component of the World Weather Research Programme (WWRP) under the World Meteorological Organization (WMO). The TIGGE (THORPEX Interactive Grand Global Ensemble) is a part of THORPEX and archives ensemble forecast data from ten global NWP centres. The data is downloaded from the archive (http://apps.ecmwf.int/datasets/data/tigge/). It is available from October 2006 for analysis. In case of NCEP, data is available from March 2007 onwards. Further details can be found in the TIGGE website (http://tigge.ecmwf.int/models.html).

The NCEP EPS data being analysed in this study is mean of the 20-member ensemble and one control run. Its horizontal resolution is T126 (0.9474°) and has 28 levels. Seven-day forecast data for the base time of 00 UTC was used for total precipitation for the period 2007–2012. Specific humidity, geopotential height, U component of wind, V component of wind and temperature used are also 7-day forecast data for the base time of 00 UTC for the period 2007–2012.
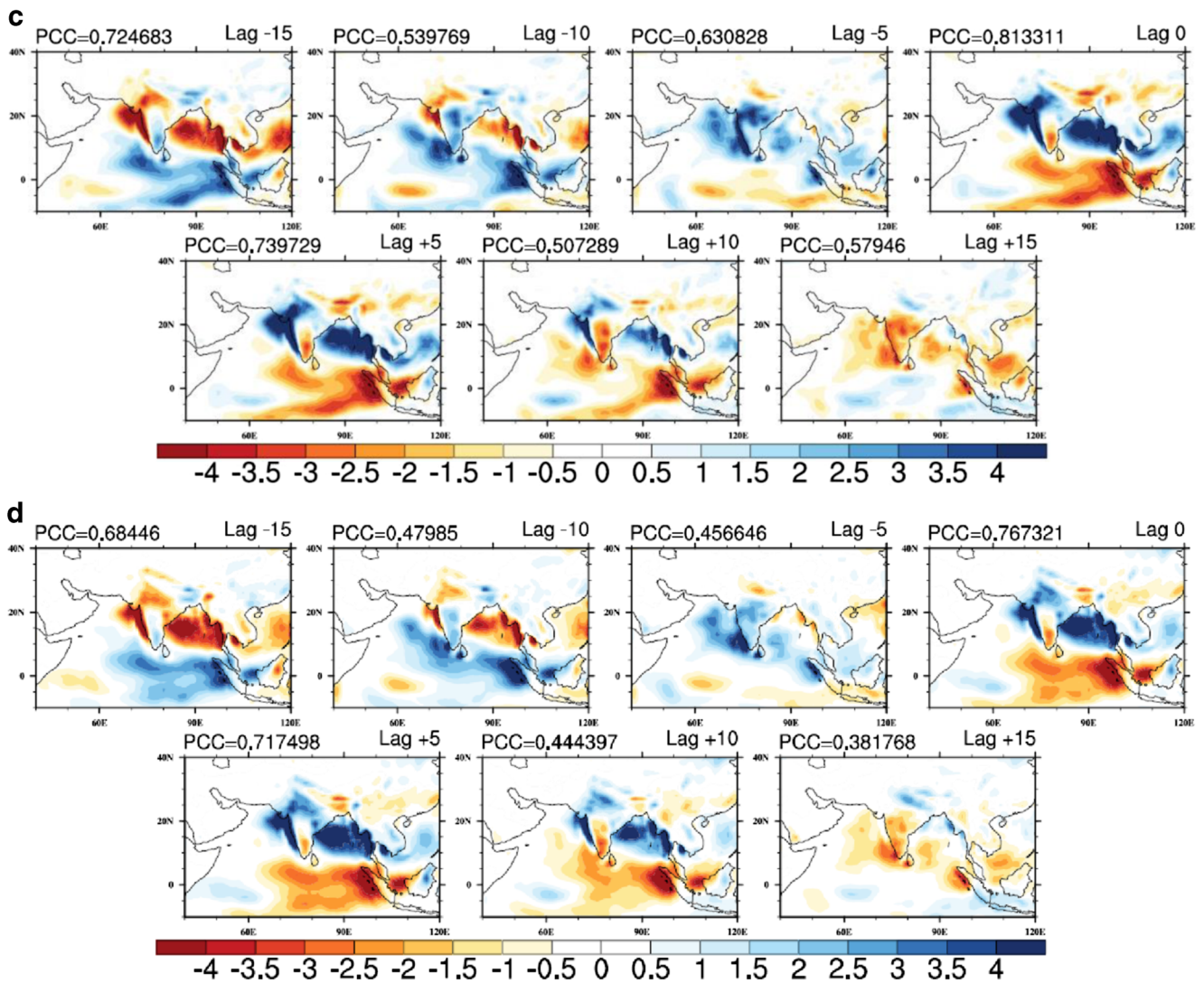
c

d

Fig. 15 (continued)

2.3 Methodology

2.3.1 Analysis with observation data

Using the TRMM 3B42 daily precipitation data, a smoothed climatology is prepared and then an anomaly time series is constructed for the period 2005–2012. Since we are investigating the MISOs, JJAS months are only considered. Power spectrum for the anomaly time series shows the dominant signals to prevail in 30–80 days periodicity. Subsequently, the anomaly time series is filtered for 30–80 days using Lanczos filter (Duchon 1979). The filter is used with 85 weights. A box over Central India (18°N–25°N, 73°E–85°E) is chosen to construct an index for active and break spell of rainfall (Fig. 1). Central India is specifically considered
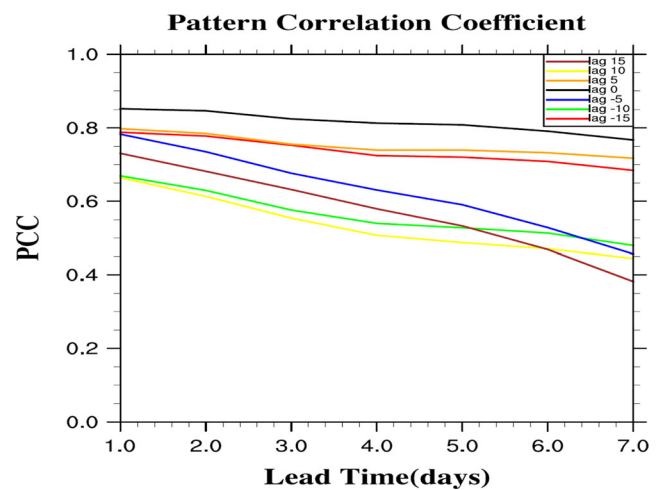

Fig. 16 Pattern correlation for active period between observation and forecast at different lags with forecast lead time

for this as it is the most homogeneous area in terms of rainfall as has been used by many earlier works (Taraphdar et al. 2010; Goswami et al. 2011; Abhik et al. 2013). The filtered anomaly is standardized by its own standard deviation, and the event of three or more than three consecutive days having greater (lesser) than +1 (−1) standard deviation is considered to be active (break) periods of rainfall. From these periods of three or more days, the central date is fixed as lag 0 and this is used to prepare the lead lag composites (Fig. 2). Separate composites are prepared for these active and break periods for different lags.

The specific humidity data from NCEP/NCAR reanalysis is used to plot the vertical structure of specific humidity (kg kg^{-1}) with respect to convection centre averaged over 75°E–83°E for both active and break period. This is also subjected to the procedure followed for precipitation; i.e. a smoothed climatology is prepared and then an anomaly time series is constructed which is filtered for 30–80 days using Lanczos filter (Duchon 1979). This filtered anomaly of specific humidity is composited for the active and break dates obtained from precipitation

analysis as explained earlier. This is done to see the evolution of specific humidity over the region of convection.

Moisture divergence is calculated using centred finite difference method with U and V component of wind along with specific humidity. The same procedure is undertaken as in case of specific humidity. The vertical structure of moisture divergence is then plotted with respect to convection centre averaged over 75°E–83°E for both active and break period.

Moist static energy is calculated using the formula:

$$S = C_{p}T + gZ + L_{v}q$$

where
C_p= 1004 J K^{-1} kg^{-1}, specific heat at constant pressure
T = air temperature (K)
g = 9.81 m s^{-2}, gravitational constant
Z = geopotential height (m)
L_v = 2.5 × 10^{6} J kg^{-1}, latent heat of vaporisation
q = specific humidity (kg kg^{-1})
Moist static energy thus calculated is then subjected to the process of computation of a smoothed climatology and then
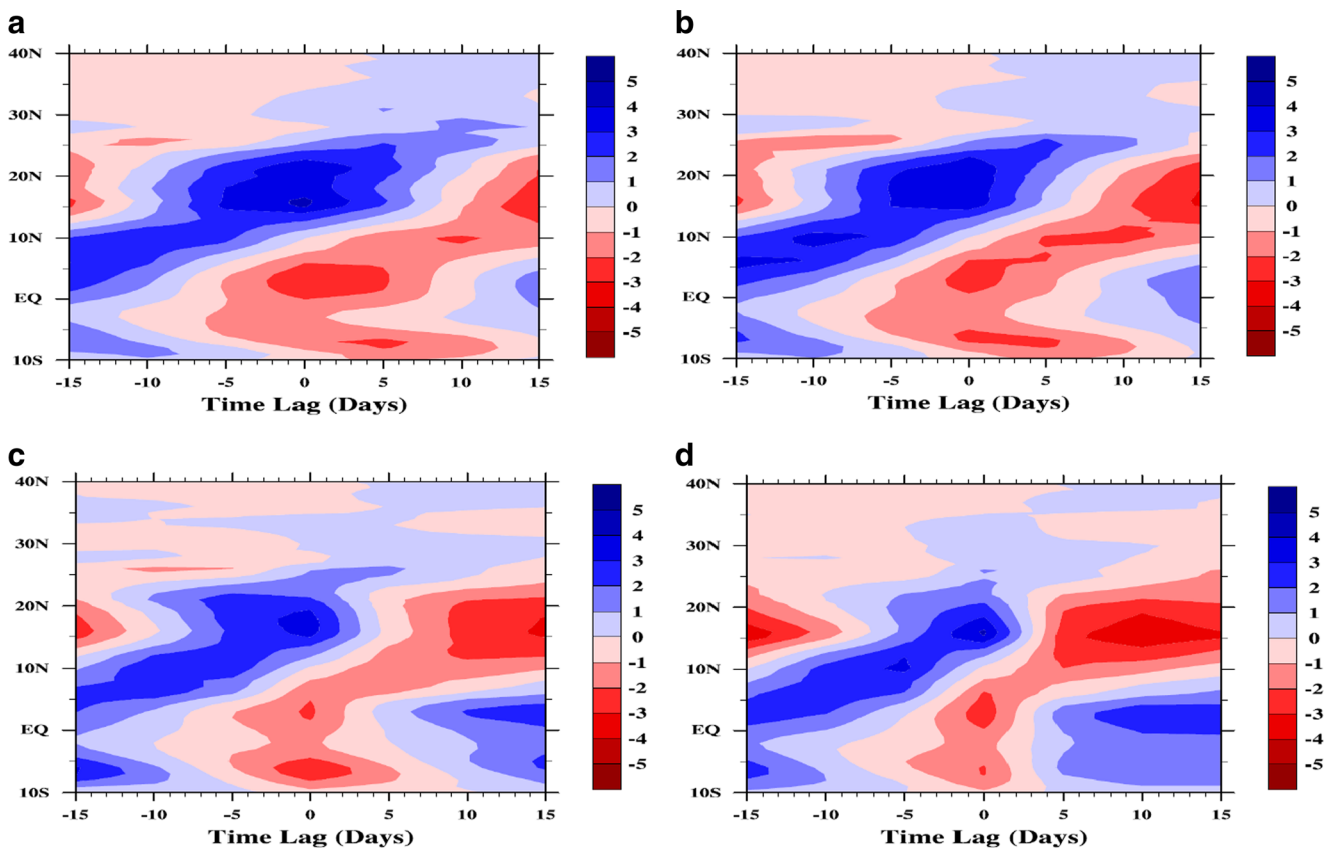

Fig. 17 Lag-latitude plot for NCEP EPS forecast rainfall anomaly averaged over 70°E–90°E for the active period for forecast lead time of **a** 24 h, **b** 48 h, **c** 96 h and **d** 168 h
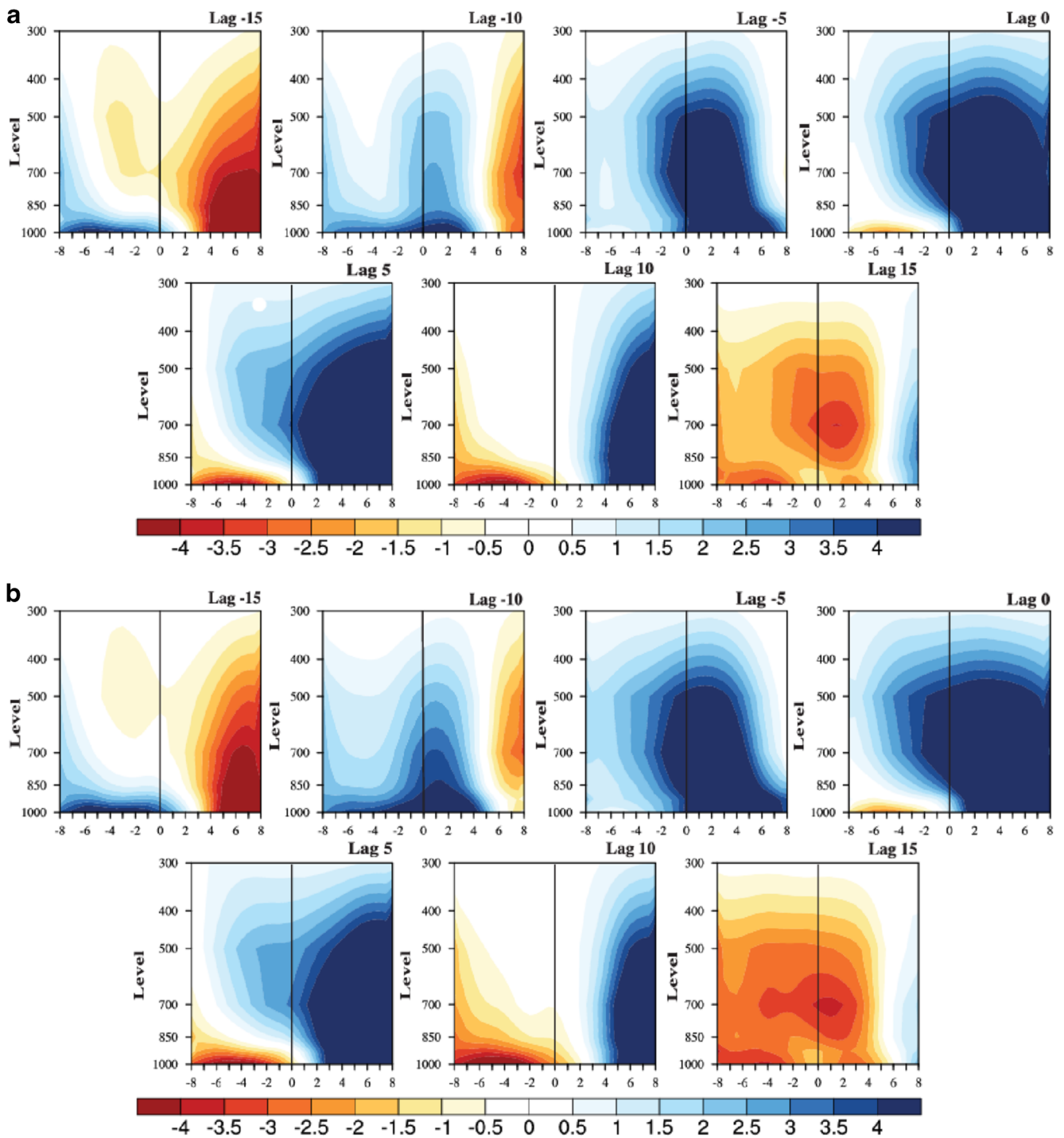
Fig. 18 Composite of meridional-vertical structure of specific humidity (kg kg^{-1}, ×10^{-4}) with respect to convection centre for active period using NCEP EPS data from **a** 24 h, **b** 48 h, **c** 96 h and **d** 168 h forecast lead time

filtered as in case of specific humidity. Here also we plot the vertical structure of moist static energy with respect to convection centre averaged over 75°E–83°E for both active and break periods.

The air temperature data from NCEP/NCAR reanalysis is used to plot the tropospheric temperature. The tropospheric temperature (TT) is the air temperature averaged between 700 and 200 hPa (Goswami and Xavier 2005). It is averaged
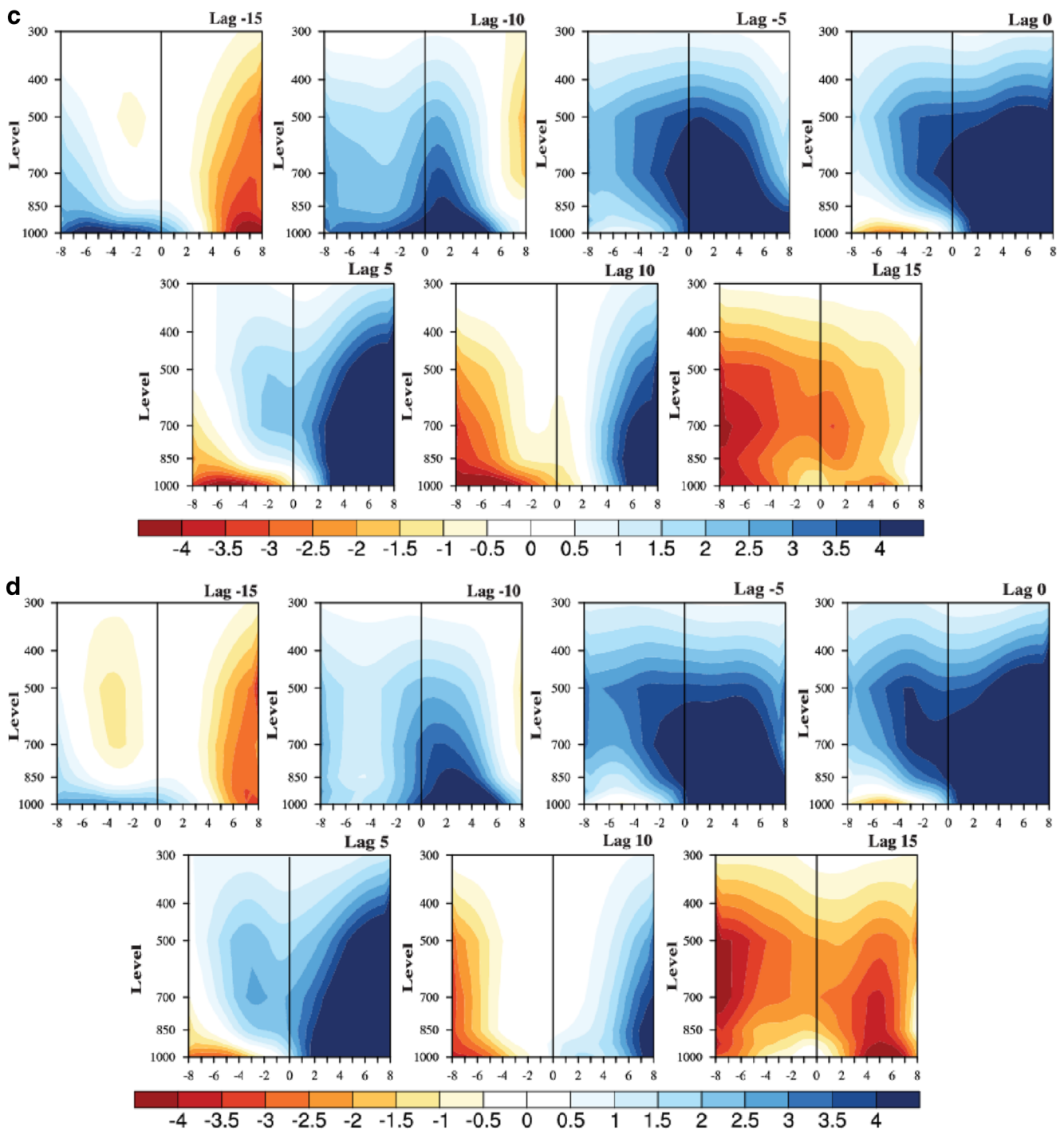
Fig. 18 (continued)

meridionally along 70°E–90°E, and the tropospheric temperature is plotted with respect to latitude. It is then analysed for the temperature gradient between the Tibetan plateau where the heat source is located during monsoon months and the cooler lower latitudes. This is an important feature of the monsoon as this heat source drives the monsoon circulation

(Webster et al. 1998). During active period, the gradient is stronger than in the break period which in turn affects the monsoon circulation and hence affects precipitation during these periods.

The wind shear between 850 and 200 hPa is also an important indicator of the strength of monsoon. Wind
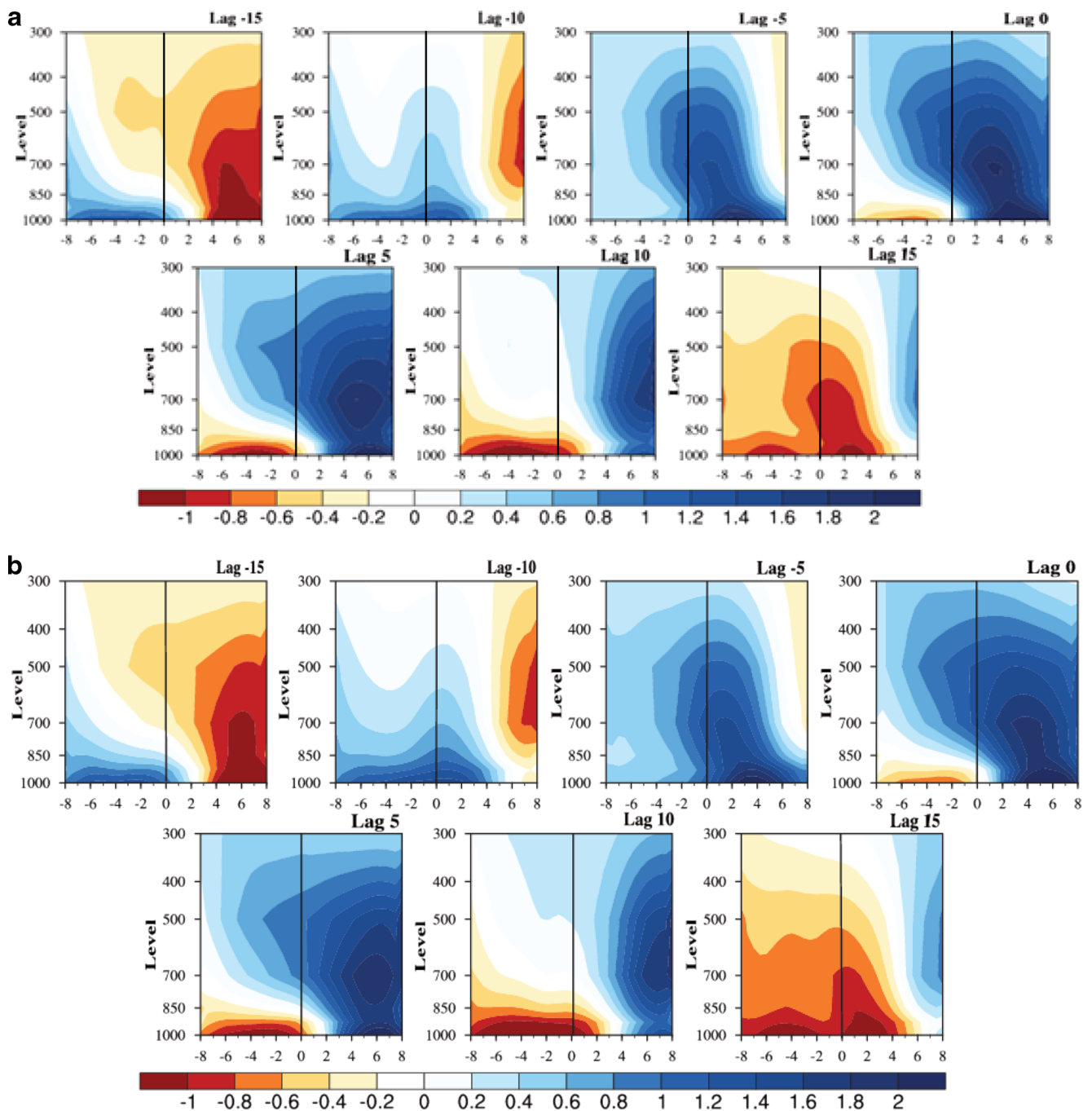
Fig. 19 Composite of meridional-vertical structure of moist static energy (kJ kg^{-1}) with respect to convection centre for active period using NCEP EPS data from **a** 24 h, **b** 48 h, **c** 96 h and **d** 168 h forecast lead time

shear is calculated by subtracting the wind at 200 hPa from wind at 850 hPa. It is then averaged meridionally along 70°E–90°E, and the shear is then plotted with respect to latitude. This is an effective way to quantify the strength of the tropical easterly jet (TEJ) which establishes itself during the monsoon over 15°N at 200 hPa. A strong easterly shear contributes to the northward propagation of MISO. This is explained later in Section 3.2.1.

The intraseasonal variability of rainfall is also assessed by calculating the variance in the TRMM rainfall data for the JJAS months for the years 2007–2012. The data is
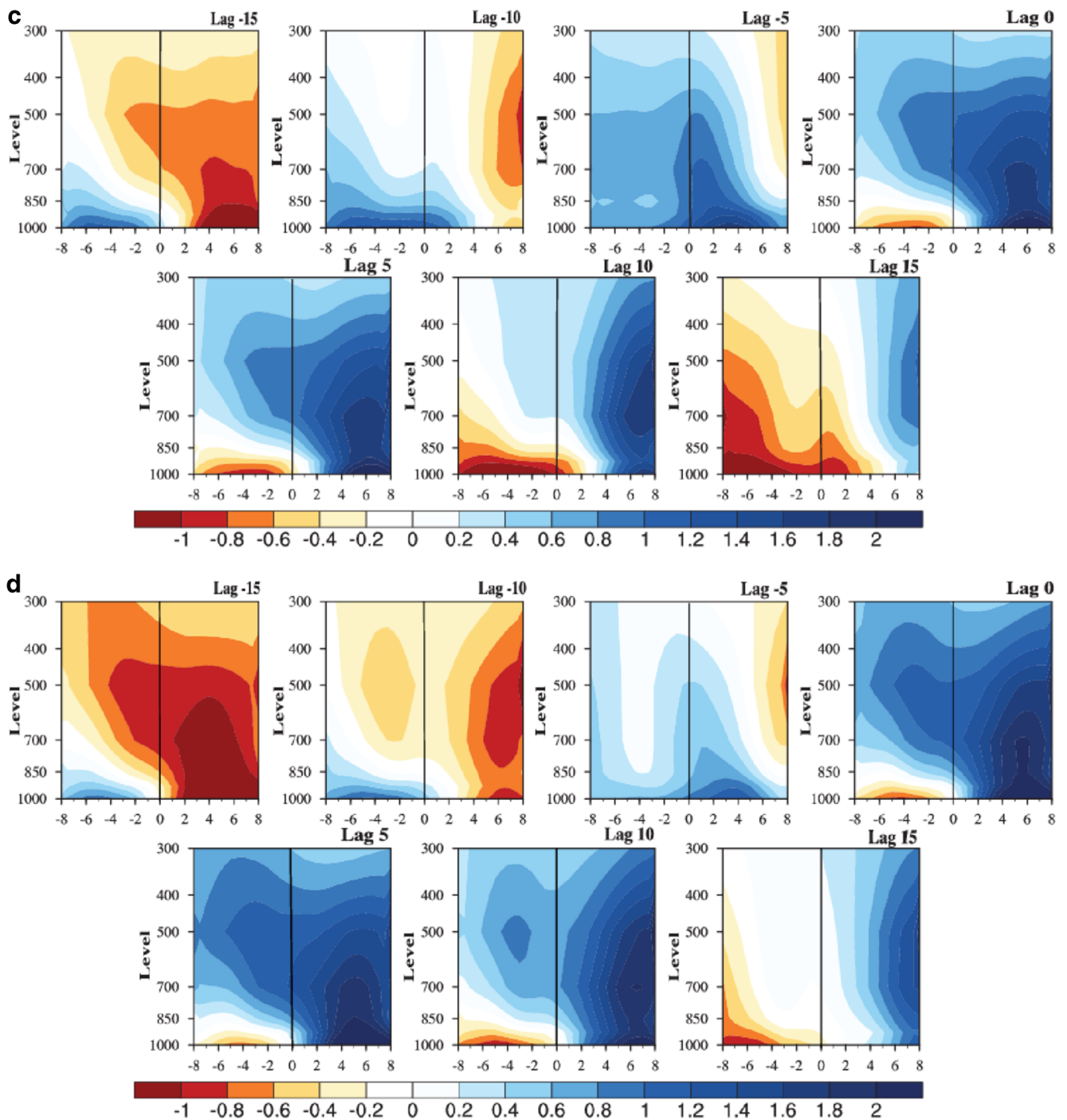
Fig. 19 (continued)

filtered for 30–80 days, and variance is calculated at each grid point. Checking for the variance captured by the model forecast will indicate whether the model is capable of simulating the deviations from the mean state or the *weather*.

To get an insight about the fidelity of EPS for good and deficient monsoon years, the forecast for the years 2007 and 2009 is evaluated considering these years as a representative of good and deficient monsoon year respectively. The Indian Meteorological Department (IMD) reported (Annual Climate
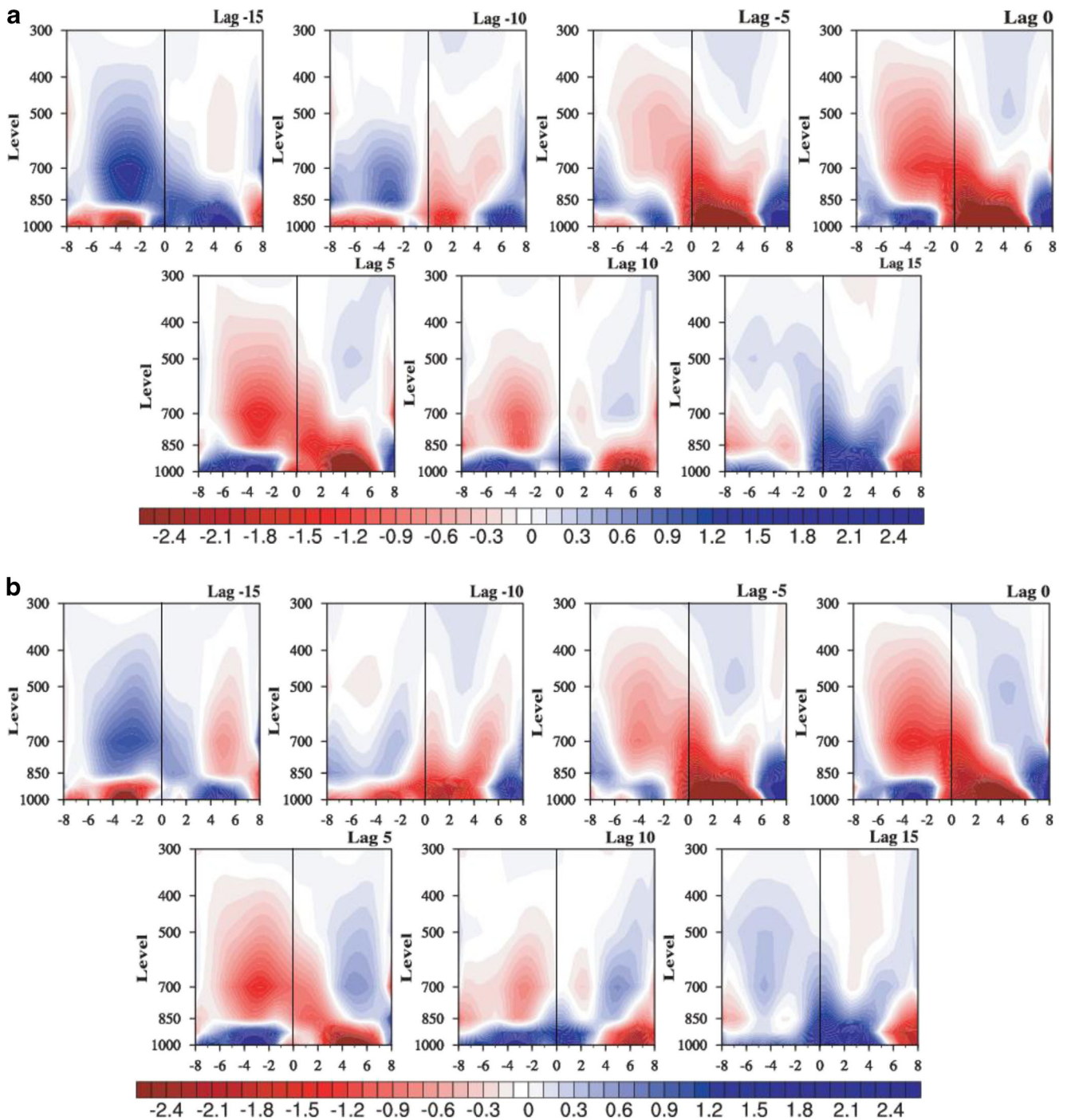
Fig. 20 Composite of meridional-vertical structure of moisture divergence (s^{-1}, ×10^{-8}) with respect to convection centre for active period using NCEP EPS data from **a** 24 h, **b** 48 h, **c** 96 h and **d** 168 h forecast lead time

Summary available from http://www.imdpune.gov.in/Clim_ RCC_LRF/Products.html) total seasonal rainfall for the year 2007 as 106 % of the long period average (LPA) and that for the year 2009 as 78 % of the LPA. The composites of rainfall anomaly are prepared for the active and break periods of 2007 and 2009.

2.3.2 Analysis with forecast data

In this section, we examine 7-day NCEP EPS forecast data for the MISOs as seen in observation. The same procedure is followed as it is done to analyse observation. First, each day's forecast precipitation is derived
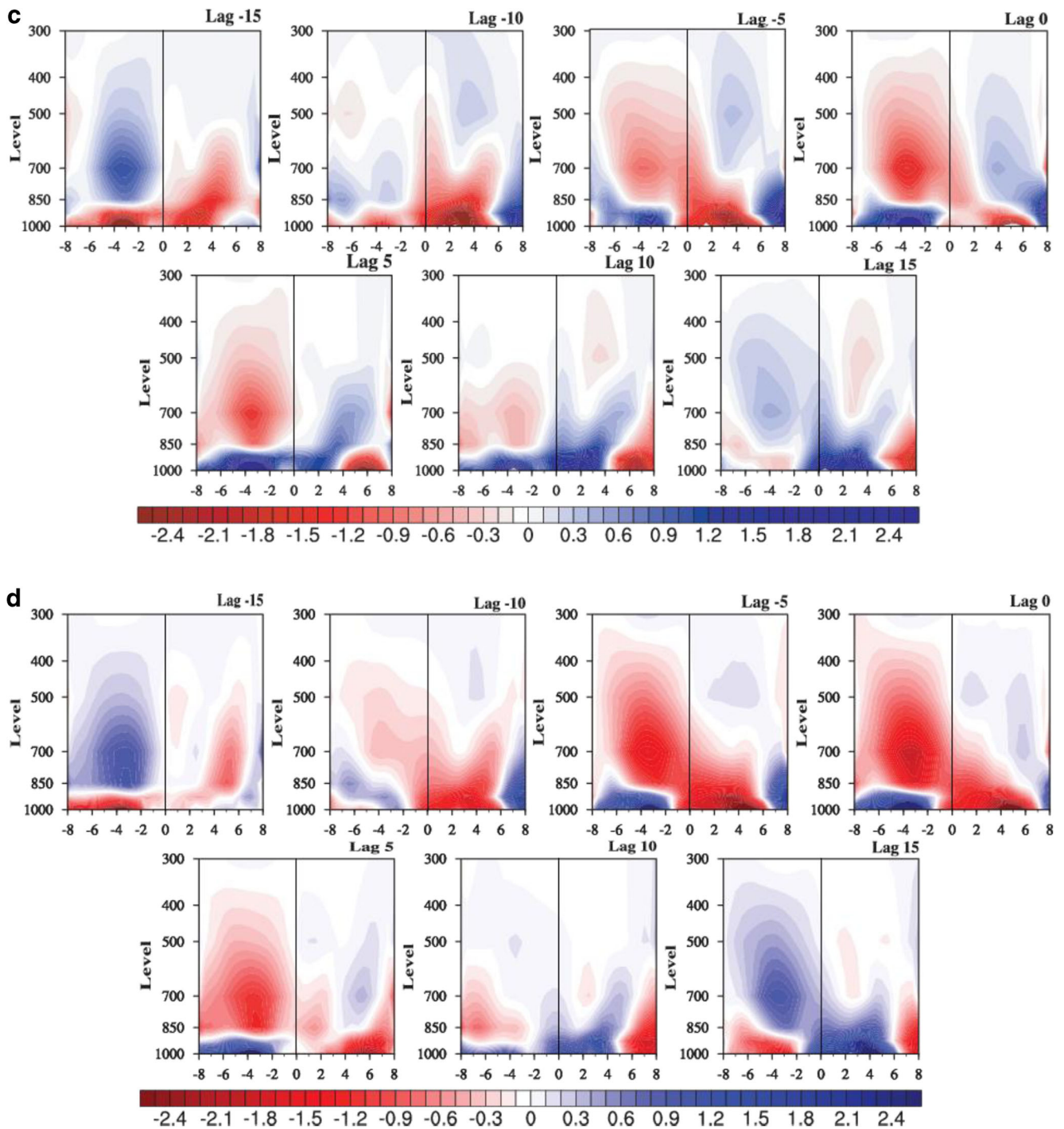
Fig. 20 (continued)

from the data of accumulated precipitation. A smoothed climatology is prepared and an anomaly $(x - \overline{x})$ time series is constructed. Subsequently, this anomaly is filtered for 30–80 days using Lanczos filter. For the active and break dates obtained from TRMM observation analysis, composites are made for the forecast data for lag −15 to lag +15 days and for all 7-day forecast. The pattern correlation is also computed for the observation and forecast rainfall anomaly composites.
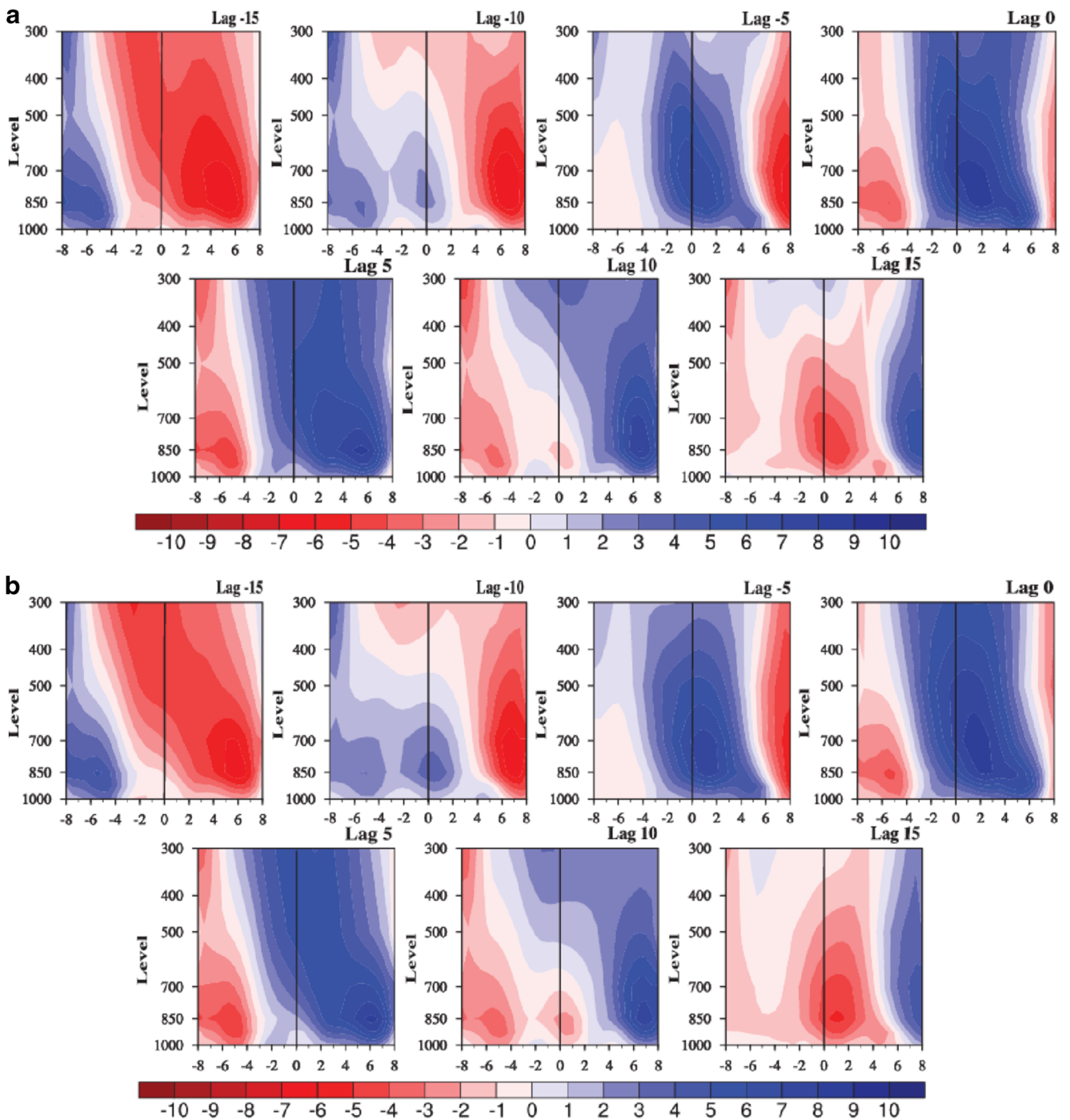
Fig. 21 Composite of meridional-vertical structure of vorticity (s^{-1}, ×10^{-6}) with respect to convection centre for active period using NCEP EPS data from **a** 24 h, **b** 48 h, **c** 96 h and **d** 168 h forecast lead time

For the vertical structure of specific humidity in the forecast, NCEP EPS data is used. Climatology is computed from it and then an anomaly time series is made for the time period 2007–2012. This is then filtered for 30–80 days using Lanczos filter. The vertical structure of specific humidity is then plotted with respect to convection centre. Moisture divergence and moist static energy are calculated for the forecast data as explained in case of observation data. The plots for these parameters are constructed using the same method as done
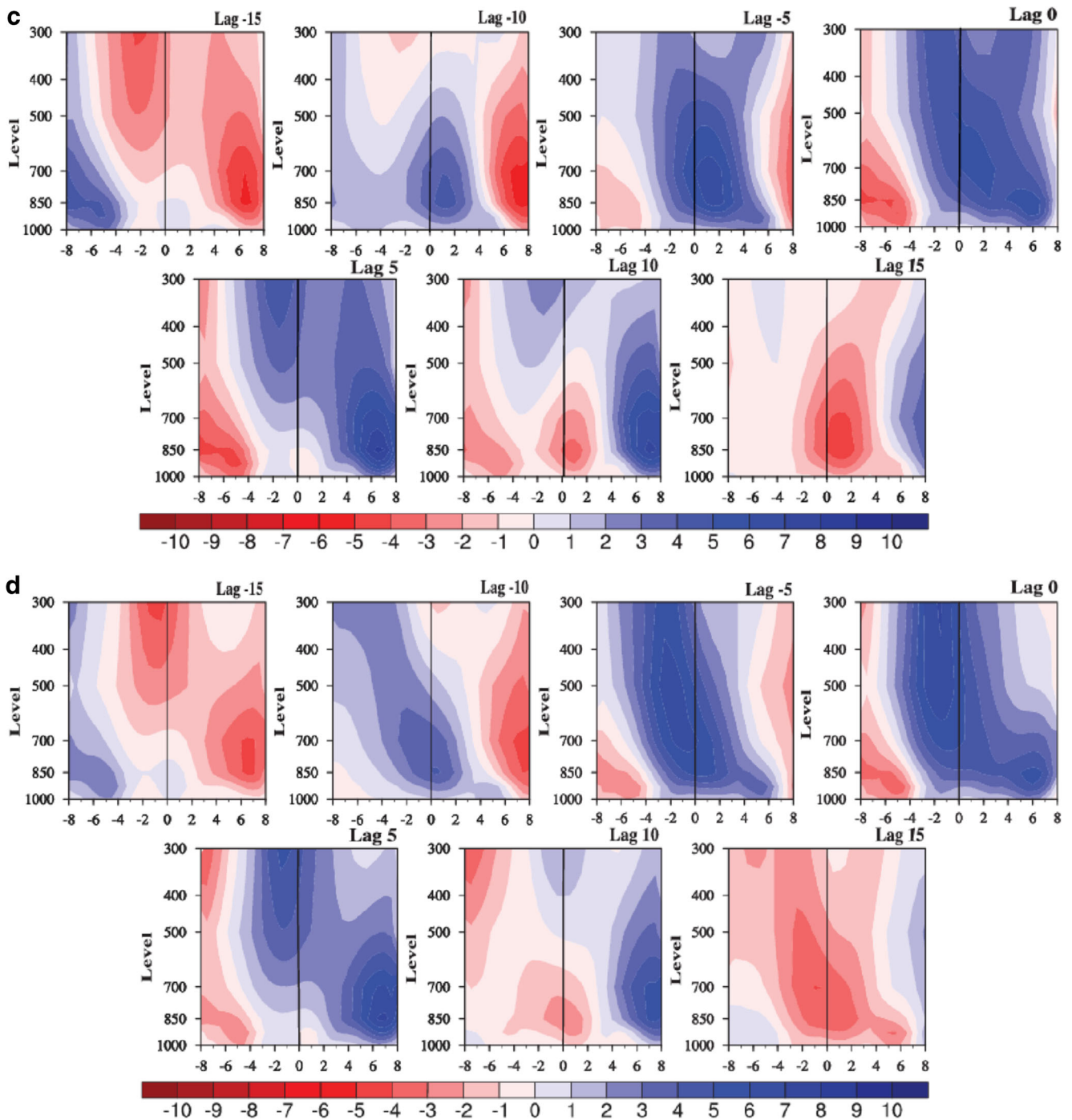
Fig. 21 (continued)

for specific humidity. The temperature data from NCEP EPS forecast is used to calculate tropospheric temperature as done in case of observations for the particular active and break dates. Wind shear is also calculated using the U and V components from NCEP EPS as in case of observations for the active and break dates

separately. Variance is calculated at each grid point for the NCEP EPS precipitation data for each lead time. It is subjected to the same procedure as in case of observation data.

Composites of precipitation anomaly are prepared for the active and break periods of good and deficient

monsoon years based on model forecast. The NCEP EPS precipitation data is used for each lead time. Pattern correlation is calculated for the above plots with respect to the observation. Also, anomaly correlation coefficient (ACC) is calculated for JJAS of all years, JJAS of sample good and deficient monsoon year namely 2007 and 2009 over central India. To quantify the model performance, the ACC is also computed for active and break days of all the years.

3 Results and discussion

3.1 Results based on observations

As described in Section 2.3.1, the rainfall events were classified into two broad groups, Active and Break periods. In the following sections, the results are discussed separately for both the groups.

3.1.1 Active period

To analyse the large-scale organization and movement of the precipitation belt over ISMR during the active period, we constructed lag composites of the precipitation anomalies from lag −15 to lag +15 (Fig. 3). The establishment of a positive anomaly band over the central Indian region and negative anomaly band over the equatorial Indian Ocean (EIO) at lag 0 conforms to the high rainfall over land during active period. The propagation of the positive anomaly from the EIO at lag −15 to the central Indian latitude at lag 0 displays the northward propagation of MISO, and it is also seen that the half cycle of MISO is resolved in lag of 15 days (Suhas et al. 2012). To get a better insight into the propagation of the precipitation belt, lag-latitude plot of rainfall anomaly averaged over 70°E–90°E for active period is shown in Fig. 4. We can clearly observe the positive anomaly to propagate from EIO region to the central Indian region with a speed of 1°day^{-1} consistent with earlier studies (Abhik et al. 2013). Hence, the large-scale organization and northward propagation of precipitation during the active period is clearly established.

Further, to examine the dynamical and thermodynamical parameters associated with precipitation, lag composites of specific humidity anomaly, moisture divergence, moist static energy and vorticity, plotted with respect to convection centre, are analysed. Figure 5
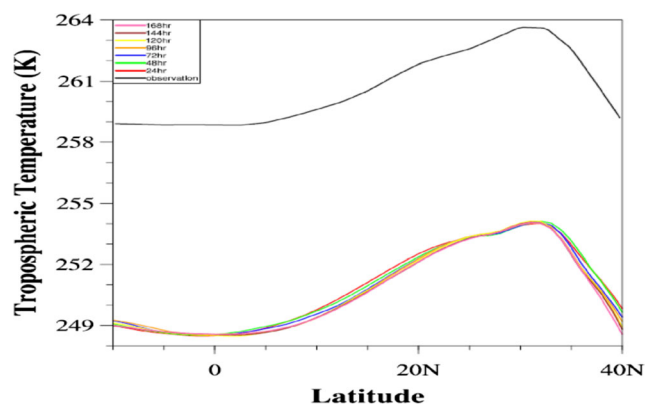

Fig. 22 Tropospheric temperature (K) averaged over 70°E–90°E for the active period (average of lag 0) using for NCEP/NCAR Reanalysis for observation and NCEP EPS forecast data for 24–168 h forecast lead time

clearly shows the evolution of positive specific humidity anomaly from shallow depth at lag −10 to the south of the convection centre which propagates northward and develops into a deep layer (reaches 600 hPa from the surface) by the time it reaches lag 0. The positive anomaly of specific humidity at lower level seen in lag −10 indicates a preconditioning of the atmosphere within the boundary layer which gradually makes the atmosphere more unstable for the deep convection to set in, which is seen at lag 0 (Abhik et al. 2013). A characteristic southward tilt can be seen in the vertical structure showing that the positive specific humidity anomaly precedes the convection. As the high positive anomaly can be seen north of the convection centre, it shows that the lower atmosphere is being pre-
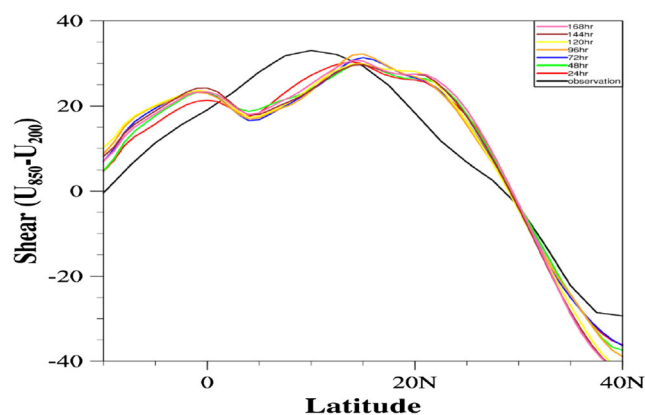

Fig. 23 Wind shear for the active period meridionally averaged over 70°E–90°E using NCEP/NCAR reanalysis data for observation and NCEP EPS forecast data for 24–168 h forecast lead time
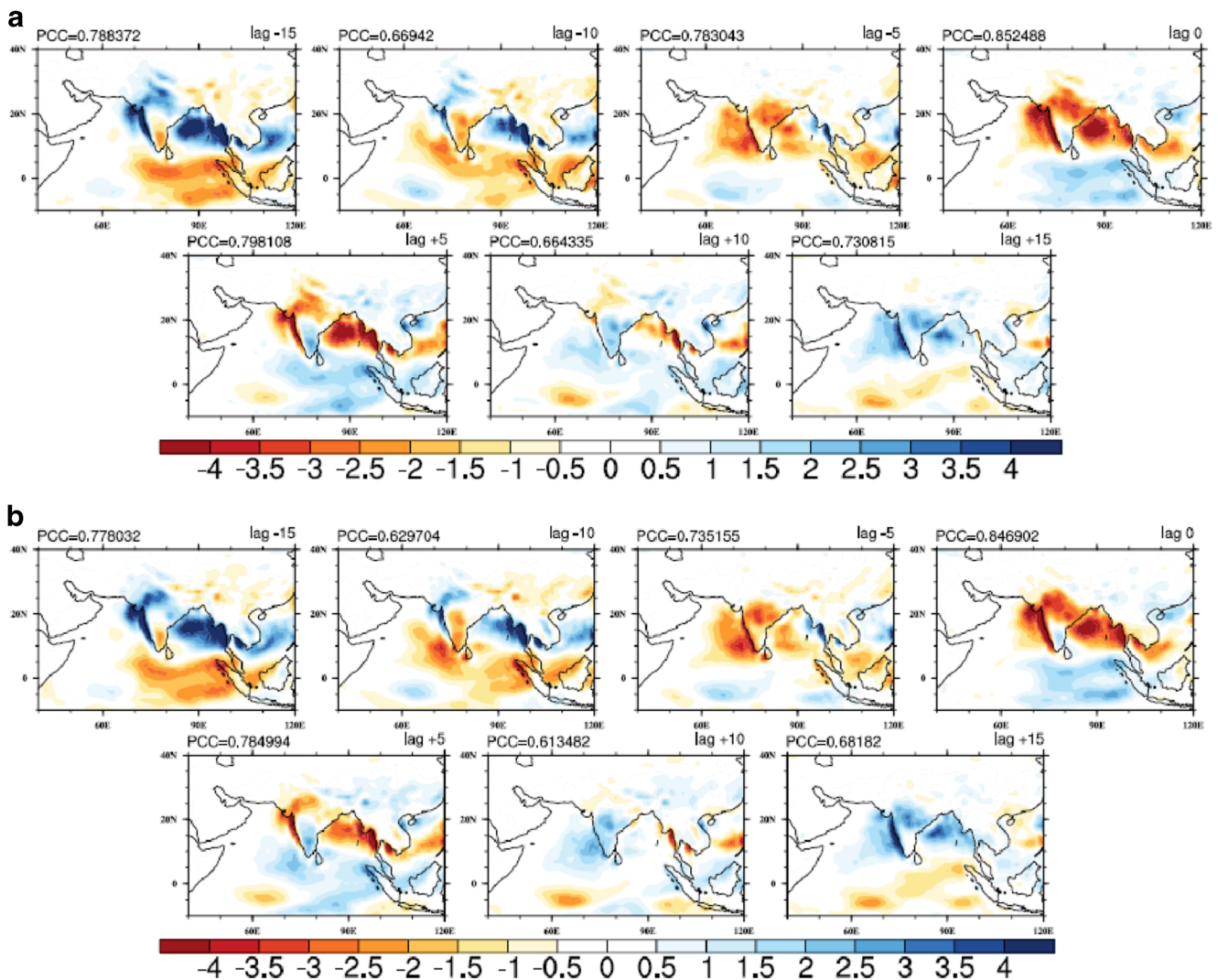
Fig. 24 Lag composite of rainfall (kg m^{-2}) during break phase from NCEP EPS data for **a** 24 h, **b** 48 h, **c** 96 h and **d** 168 h forecast lead time

conditioned which causes the shift of the convection centre to the north. Hence, this southward tilt is an important feature which drives the convection northward. These features are also observed in moist static energy (Fig. 6) and moisture divergence (Fig. 7). Deep moisture convergence extending to 700 hPa and positive moist static energy up to 600 hPa shows favourable conditions for convection. The northward propagation and the deepening of the layer at lag 0 to about 600 hPa are clearly observed. From this, we can say that the instability of the atmosphere is very high and extends through a deep column. The strong equivalent barotropic vorticity structure is seen (Fig. 8) north of the convection centre that assists the northward shift of the moisture convergence and thus helps

to move the organized convection northward (Jiang et al. 2004).

3.1.2 Break period

A negative rainfall anomaly for at least 3 consecutive days over central India with respect to the central India precipitation index marks the break phase of monsoon. Similar analysis for break period is conducted as in Section 3.1.1. The lag composite of rainfall anomaly clearly shows the northward propagation and establishment of large-scale negative anomaly over central India at lag 0 (Fig. 9). The northward propagation of rainfall anomaly is further established in the lag-latitude plot (Fig. 10) which shows the progress of the negative
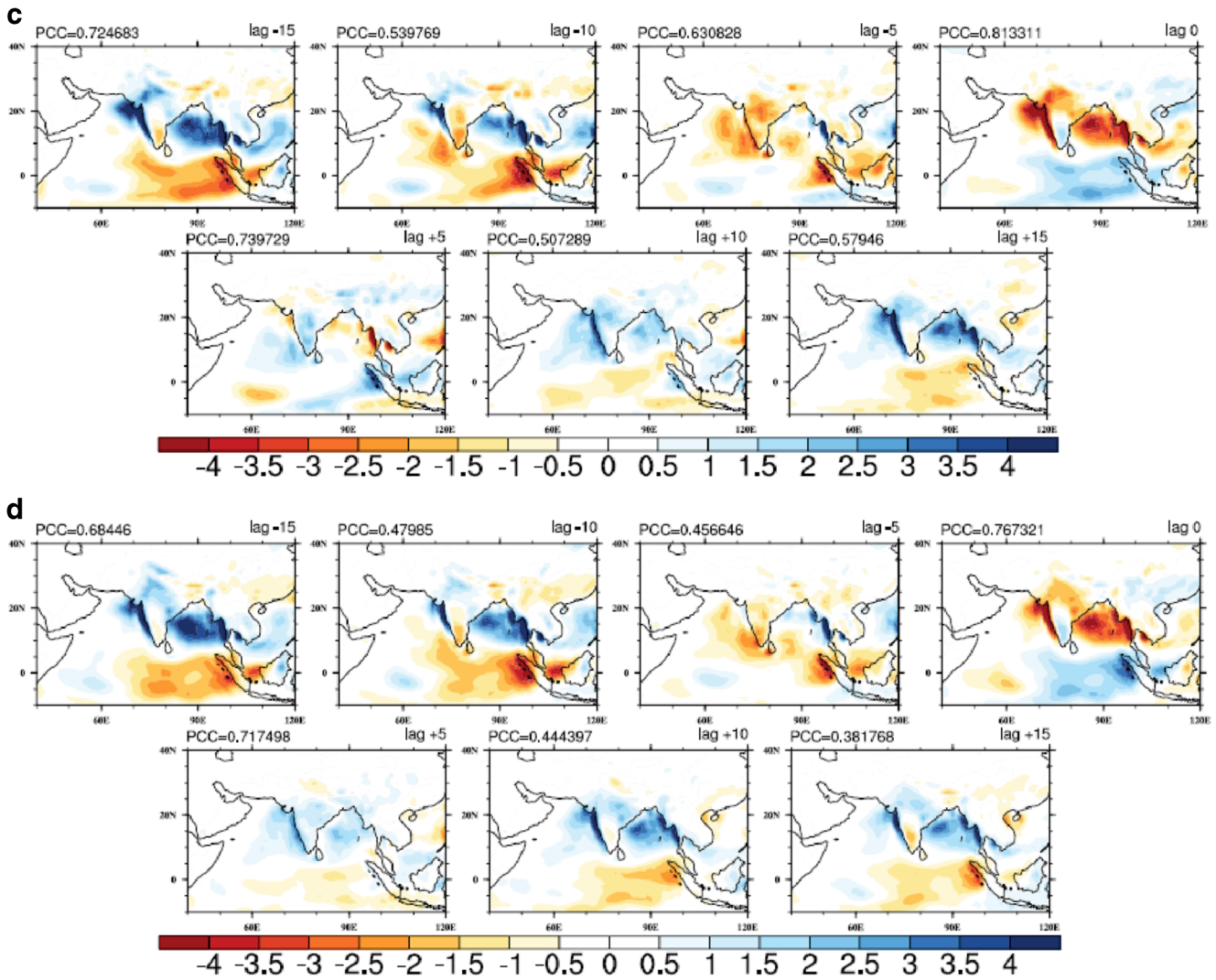
Fig. 24 (continued)

anomaly band from EIO to about 25°N with a speed of 1°day^{-1}.

The parameters associated with the thermodynamical and dynamical aspects of precipitation exhibits similar behaviour with contrasting signal as compared to active period. The evolution of negative specific humidity anomaly starts building up from boundary layer at lag −10 to the south of the convection centre and this as such propagates northward and develops into a deep dry layer (reaches 500 hPa from the surface) by the time it reaches lag 0 as evident from Fig. 11. A negative anomaly of specific humidity is indicative of drier atmospheric column and weaker or suppressed convection. This fact is further strengthened in the evolution of moist static energy and moisture divergence shown in Figs. 12 and 13 respectively. Due to low moisture
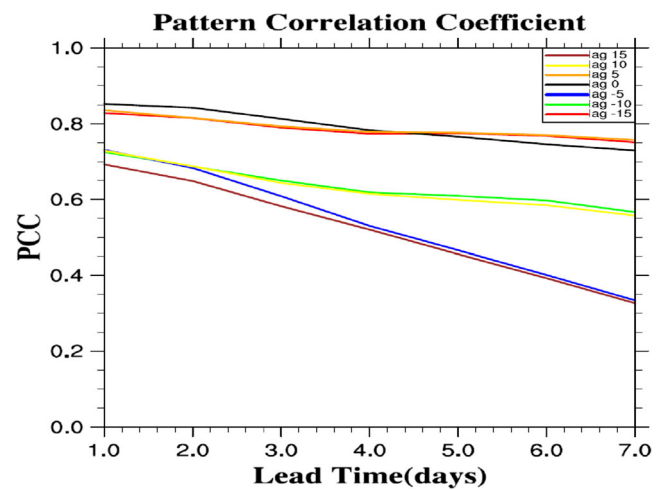

Fig. 25 Pattern correlation for break period between observation and forecast at different lags with forecast lead time
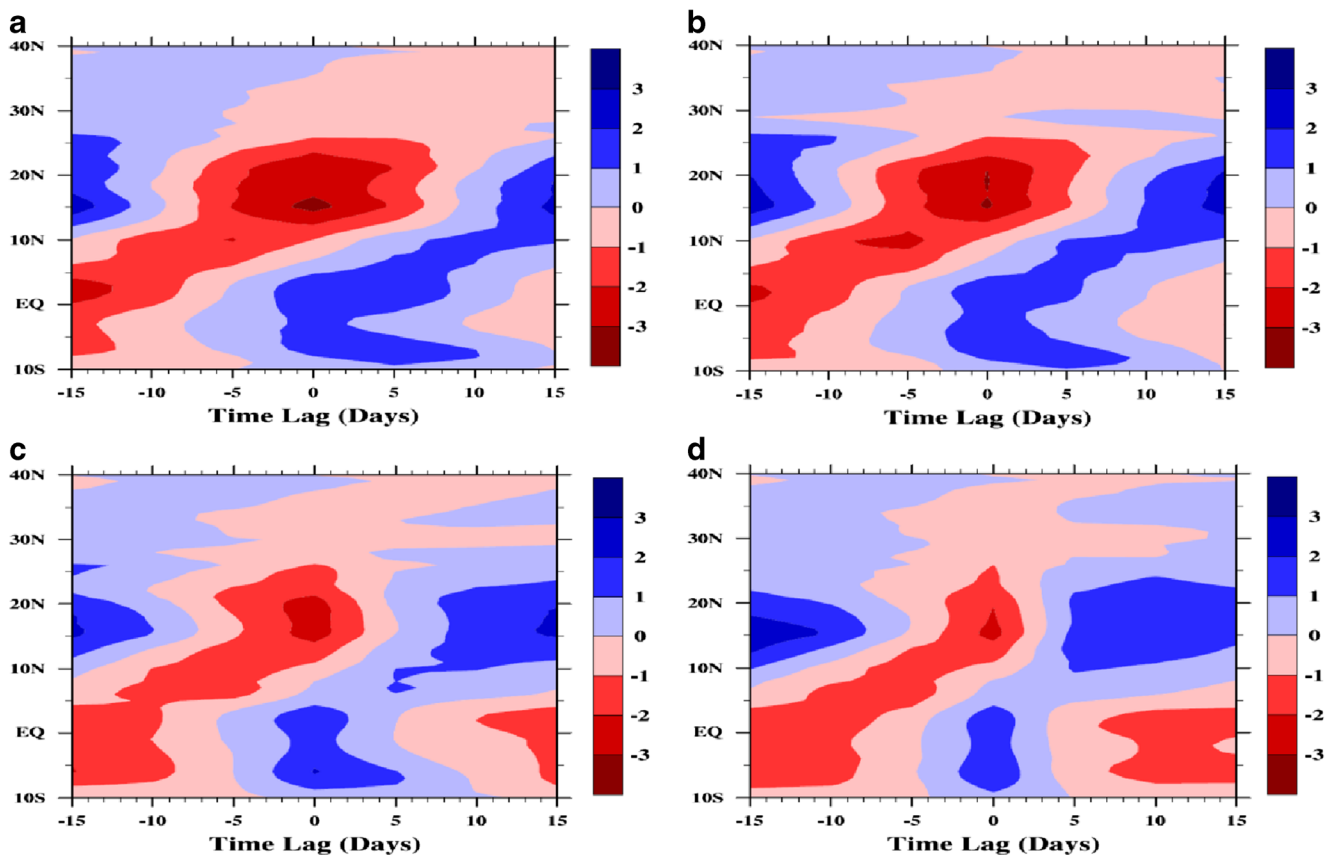
Fig. 26 Lag-latitude plot for NCEP EPS forecast rainfall anomaly averaged over 70°E–90°E for the break period for forecast lead time of **a** 24 h, **b** 48 h, **c** 96 h and **d** 168 h

availability, the moist static energy or the moist insta-bility shows anomalously low values (Fig. 12) signify-ing suppressed convection phases. Figure 13 shows dominant low-level divergence within boundary layer which causes hindrance to moist convection. The lower level divergence is evident from lag −5 to lag +10. Thus, the break phase of the Indian monsoon is charac-terized with lower level persisting divergence observed up to 700 hPa and a deep layer of negative moist static energy inhibiting convection. Anomalously negative vor-ticity is noted throughout the troposphere (Fig. 14), sug-gesting subsidence over the region and further inhibiting convergence.

3.2 Study based on NCEP EPS forecast data

The features discussed above for different aspects of MISO is analysed for NCEP EPS forecast data in the following sections. We would like to see how well and the extent to which the EPS forecast data is able to reproduce the observations. The composites for various parameters are done for all lead times from 24 to 168 h but for the current discussion 24, 48, 96 and 168 h lead times are provided.

3.2.1 Active period

To inspect whether the essence of MISO in the form of its organization and propagation is captured by the NCEP EPS forecast data, lag composite of rainfall anomaly was constructed as done for observation data. Observing Fig. 15a–d we can say that, generally, the structure of the rain bands and the northward propaga-tion of the ISO are well captured by the EPS forecast data. However, Fig. 15c, d shows that the model fore-cast produce stationary pattern at lag 0, lag 5 and lag 10 days, where more rainfall is dumped over head Bay of Bengal and the propagation slows down. Based on the pattern correlation between observation and forecast, it is seen (Fig. 16) that lag 0, lag 5 and lag 15 are well
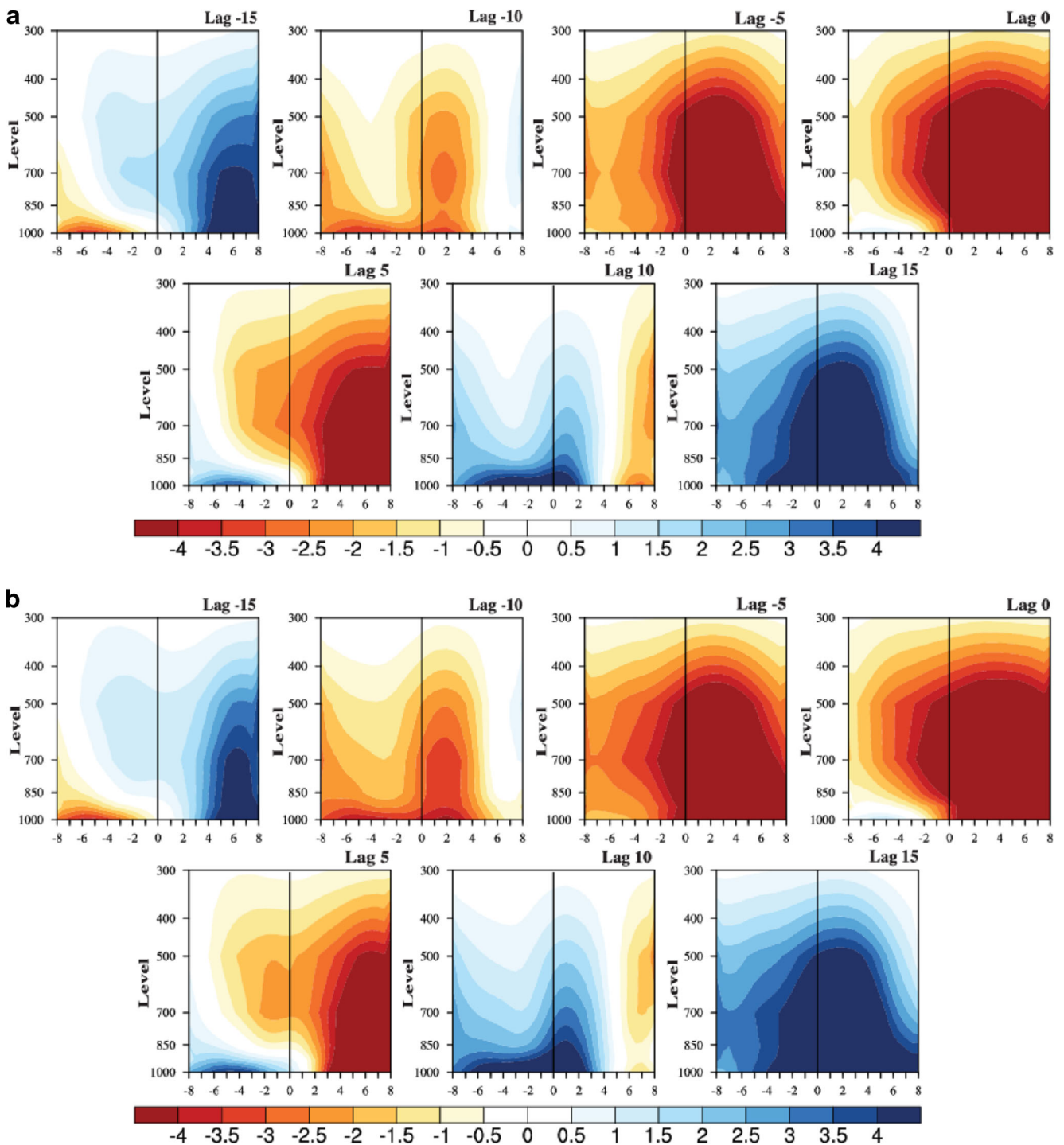
Fig. 27 Composite of meridional-vertical structure of specific humidity (kg kg^{-1}, ×10^{-4}) with respect to convection centre for break period using NCEP EPS data from **a** 24 h, **b** 48 h, **c** 96 h and **d** 168 h forecast lead time

captured by EPS even up to a lead time of 168 h (7 days). Up to 96 h (4 days), all lags maintain correlation greater than 0.5. The northward propagation is

further asserted in the lag-latitude plot (Fig. 17), where we can see the positive anomaly (blue) band moving northwards. After 96 h lead time, the extent of
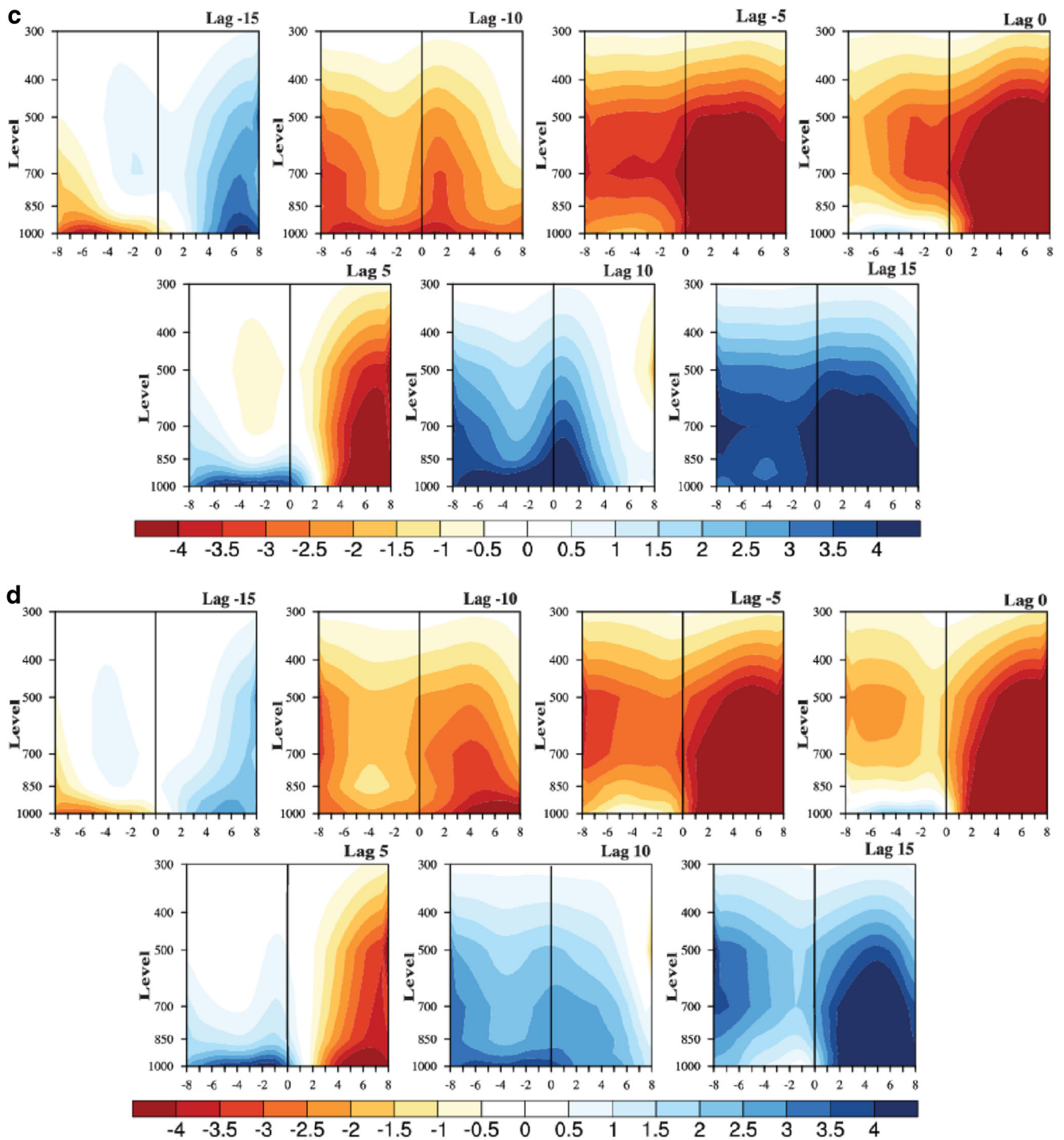
Fig. 27 (continued)

propagation limits itself to 20°N as opposed to 25°N seen in the observation data and this is consistent with what has been showed in Fig. 15c, d.

Coming to the thermodynamical and dynamical aspects, lag composite specific humidity anomaly with respect to convection centre for forecast data is constructed in Fig. 18a–d. The evolution of positive anomaly from lag −10 and its northward movement is seen even up to 168 h forecast lead time. However, the characteristic tilt of the moisture column is not seen after
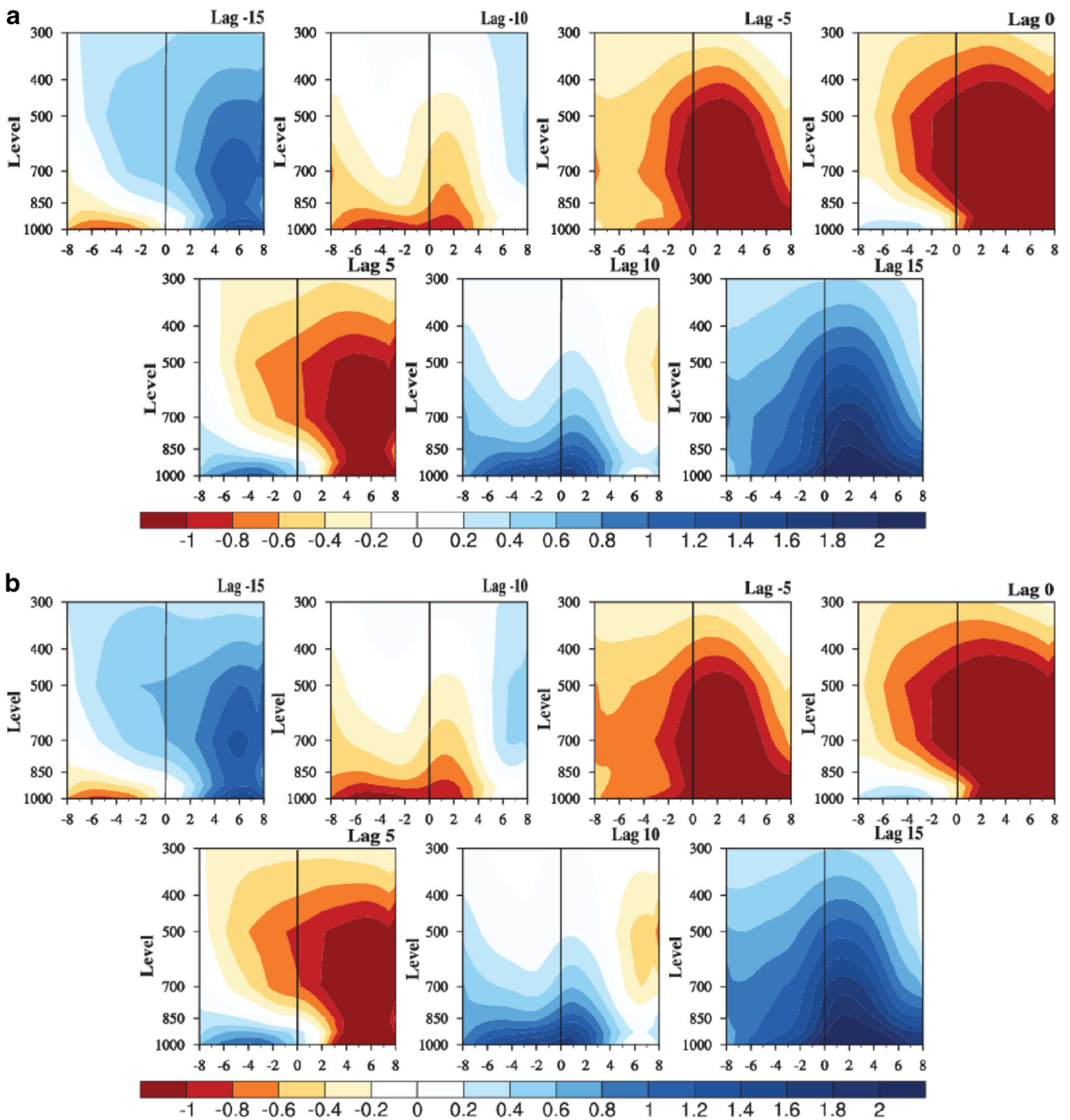
Fig. 28 Composite of meridional-vertical structure of moist static energy (kJ kg⁻¹) with respect to convection centre for break period using NCEP EPS data from **a** 24 h, **b** 48 h, **c** 96 h and **d** 168 h forecast lead time

96 h forecast lead time. This may be the cause of stagnation of the northward propagation beyond 20°N after 96 h lead time observed in the lag-latitude plot (Fig. 17). Also, the magnitude reduces after 96 h forecast lead time. The depth of the moisture column is

well captured. It goes up to 600 hPa matching with the observation implying high convective instability in the column. It is to be noted that at lag 0 the positive anomaly of specific humidity is found to have been developed more northward of the convection centre than
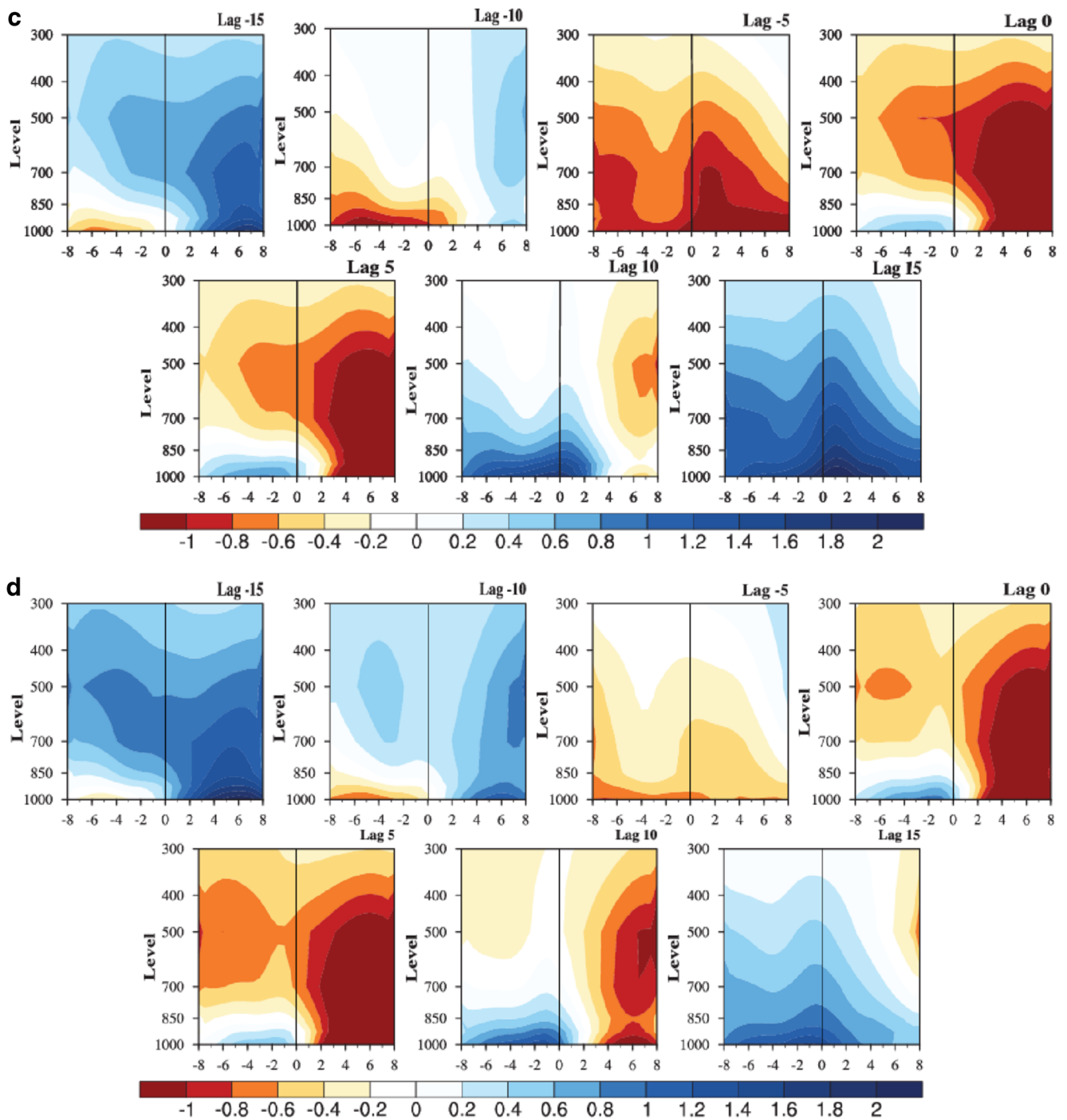
Fig. 28 (continued)

in the observation. The moist static energy also conforms to the pattern of specific humidity anomaly. The northward propagation and depth of the column is well captured as seen in Fig. 19, but the southward tilt of the column is missing from 96 h lead time. Also, the moisture convergence observed in Fig. 20 shows fairly good replication of observation at all lead times in terms of magnitude and propagation but here also after 96 h, the depth of convergence decreases; that is, the moisture convergence becomes shallower than the
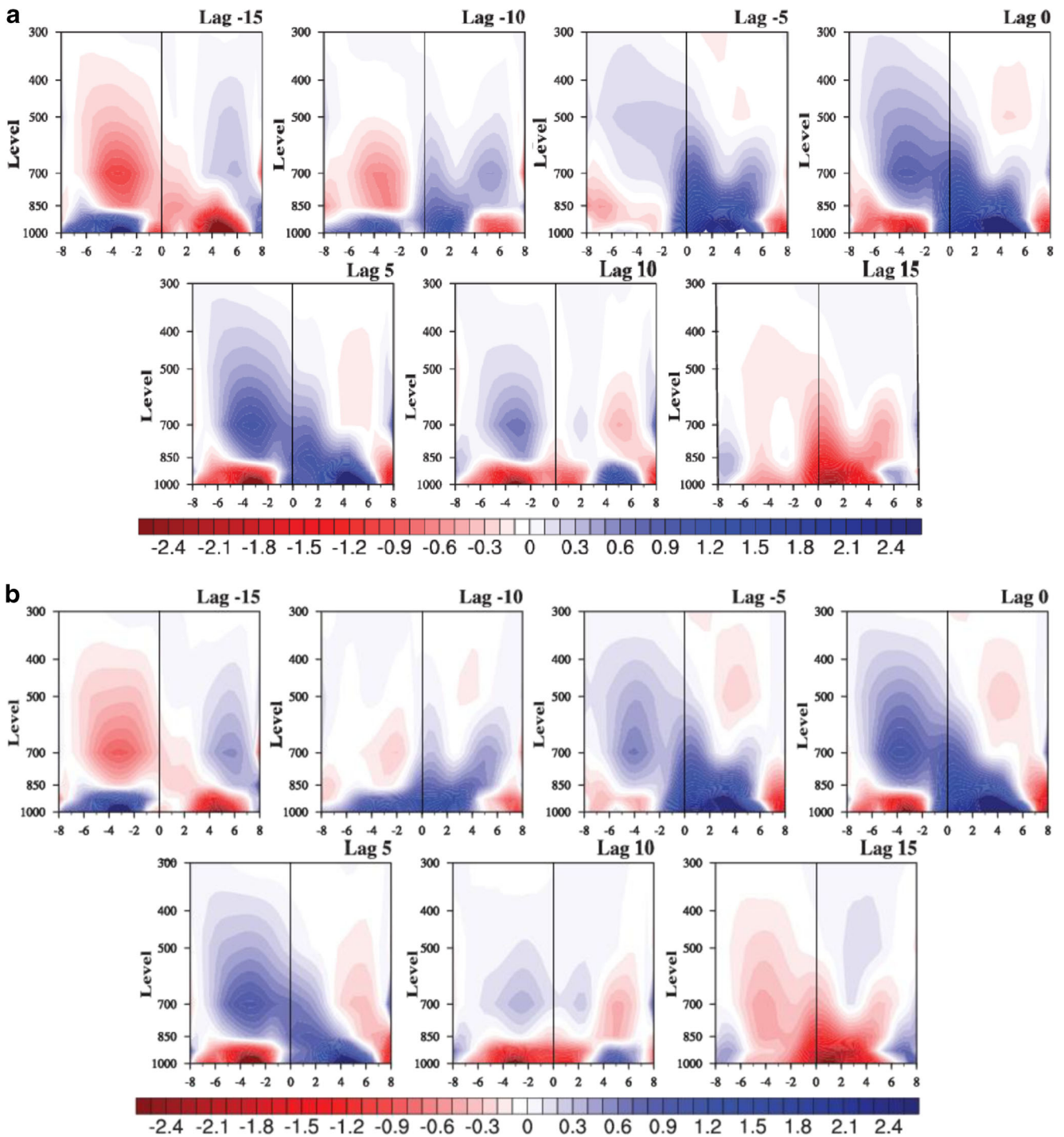
Fig. 29 Composite of meridional-vertical structure of moisture divergence (s^{-1}, $\times 10^{-8}$) with respect to convection centre for break period using NCEP EPS data from **a** 24 h, **b** 48 h, **c** 96 h and **d** 168 h forecast lead time

observation. The positive barotropic vorticity which helps in the northward shift of the convection system is also seen to be reasonably well captured by the EPS data seen in Fig. 21a–d. However, a decrease in magnitude is seen from 96 h onwards. Thus, we can note that the forecast deviates more from 96 h lead time onward. The challenge is to enhance the model fidelity to capture the observed anomalies even beyond 4 days.
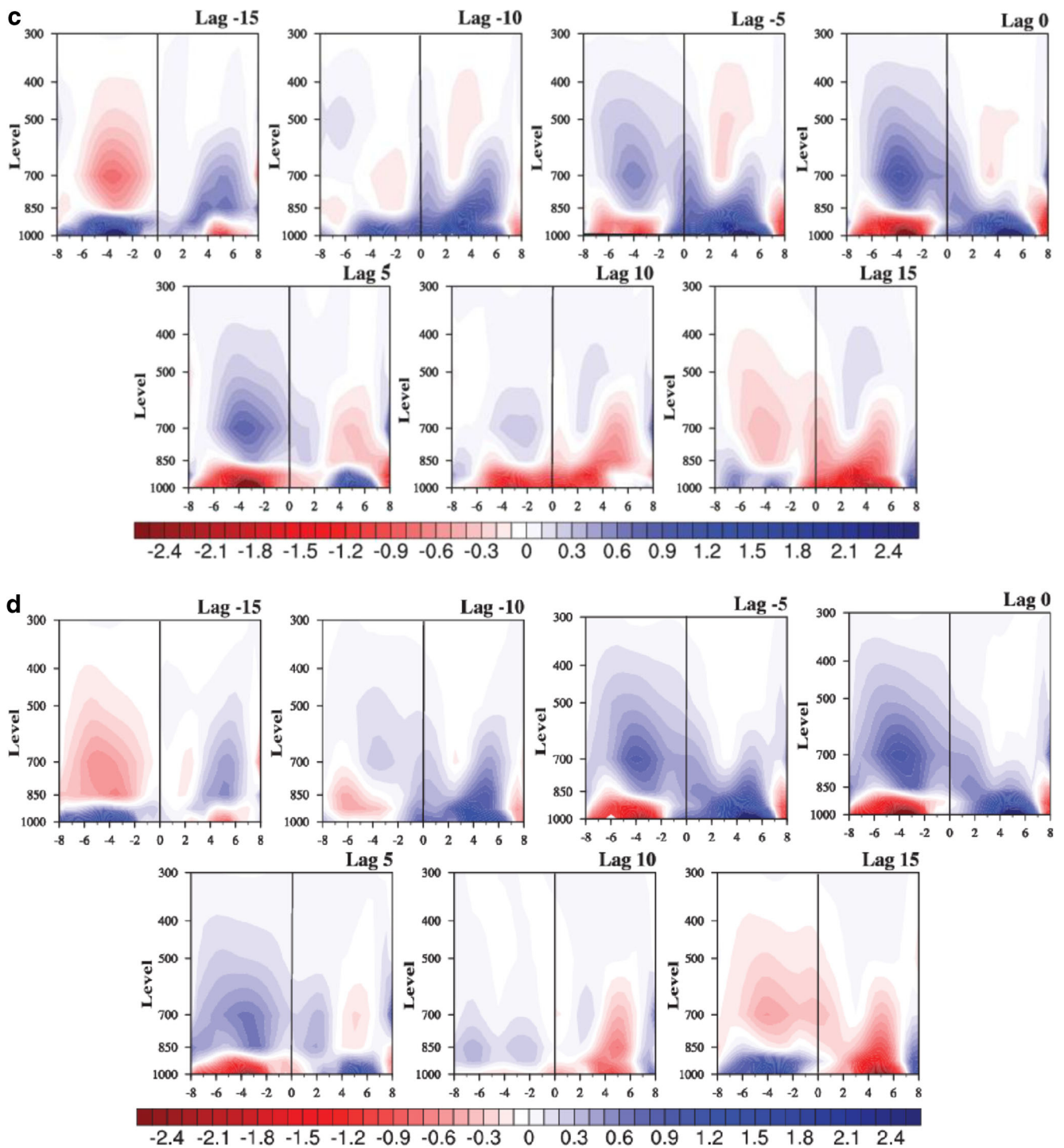
Fig. 29 (continued)

The monsoon circulation is dependent on the tropospheric temperature gradient caused by elevated temperatures in Tibetan plateau region (Webster et al. 1998). The tropospheric temperature pattern for the active period is observed in Fig. 22. It shows higher values at 30°N–35°N which is over the Tibetan Plateau region and lower temperature at over the equatorial Indian Ocean (0°S–10°S) with a steep gradient. This is a
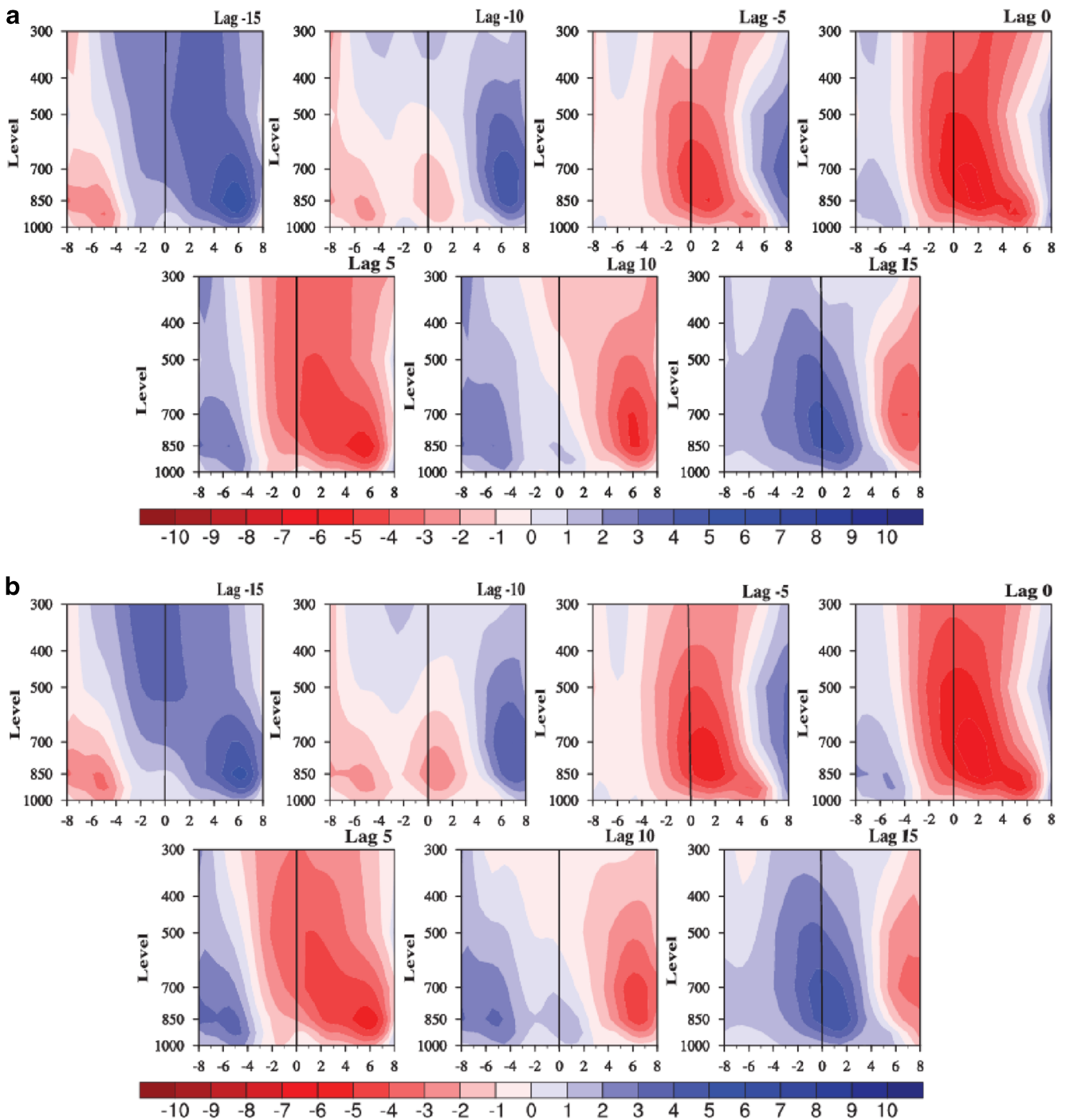
Fig. 30 Composite of meridional-vertical structure of vorticity (s^{-1}, $\times 10^{-6}$) with respect to convection centre for break period using NCEP EPS data from **a** 24 h, **b** 48 h, **c** 96 h and **d** 168 h forecast lead time

favourable condition for the monsoon. The forecast for various lead times captures the gradient but not the magnitude. Thus, we can say that the model captures the heat distribution in the troposphere but with a certain bias.

A high easterly wind shear between 850 and 200 hPa indicates a strong tropical easterly jet which enhances the low-level monsoon circulation, bringing moisture laden winds to the Indian landmass. Figure 23 shows the wind shear for active days averaged over 70°E–
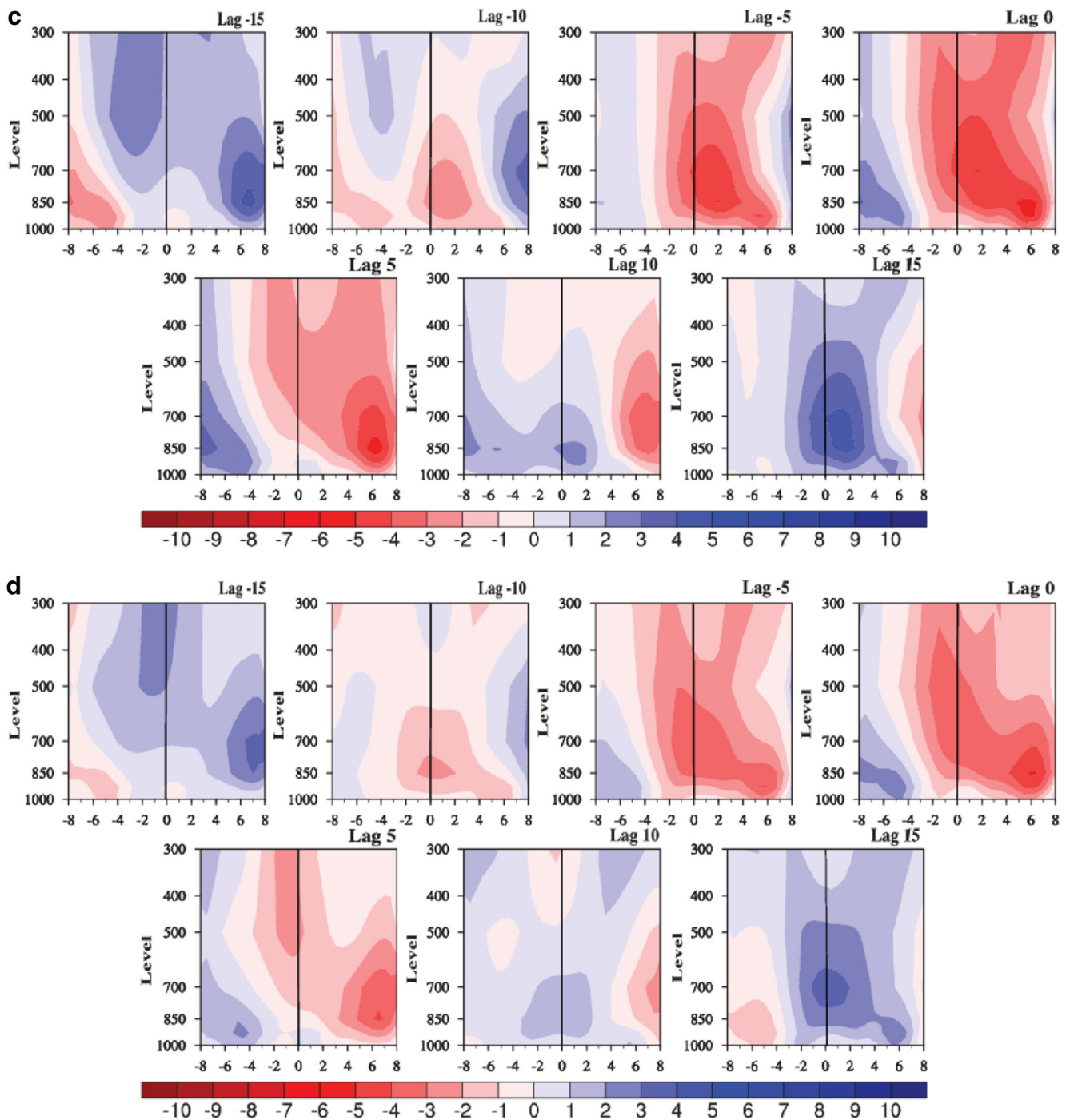
Fig. 30 (continued)

90°E. The high wind shear at 5°N–15°N clearly shows the presence of a strong tropical easterly jet. According to Jiang et al. 2004, a strong easterly shear leads to the formation of a barotropic vorticity north of the convection which is also evident from Fig. 21a–d and this in turn leads to the northward shift of moisture convergence in the boundary layer. Thus, the northward propagation of convection is facilitated. The forecast shows a considerable agreement with the observation for all lead times.
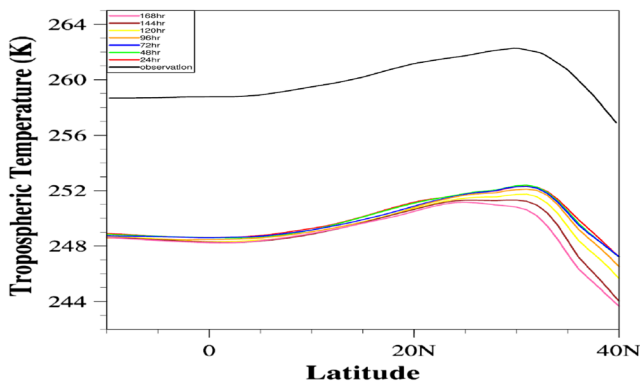
Fig. 31 Tropospheric temperature (K) averaged over 70°E–90°E for the break period (average of lag 0) using NCEP/NCAR Reanalysis for observation and NCEP EPS forecast data for the period 2007–2011 for 24–168 h forecast lead time

3.2.2 Break period

Similar analysis is conducted for investigating the break phase of monsoon as captured by the NCEP EPS forecast data. The lag composite of rainfall from NCEP EPS forecast with forecast lead time for break period is shown in Fig. 24a–d. We can observe that the structure of the rain bands and the northward propagation of the ISO are well captured by the EPS forecast data. The break phase is better captured than the active phase. The pattern correlation between observation and forecast at lag 0, lag 5, lag −15 and lag 10 are well captured (Fig. 25) by EPS even up to lead time of 168 h (7 day). But for other lags, the pattern correlation falls below 0.5 after 96 h (4 day) forecast lead time. The lag-latitude plot shown in Fig. 26a–d fairly agrees with the

observation up to 96 h lead time. Beyond this, the propagation of anomaly is stagnated at 20°N.

Now analysing various thermodynamical and dynamical parameters for the break phase, we observe the evolution of specific humidity with respect to convection centre for forecast data as shown in Fig. 27a–d. The evolution of negative anomaly from lag −10 to lag +10 is shown. Its northward movement with respect to the centre of suppressed convection is seen even up to 168 h forecast lead time. But the characteristic tilt of the moisture column is not seen from 96 h forecast lead time. This may be the cause of stagnation of the northward propagation after 96 h lead time observed in the lag-latitude plot (Fig. 26). Also, the magnitude reduces after 96 h forecast lead time. The depth of the column is well captured. It goes up to 600 hPa as in case of the observation. It is to be noted that at lag 0 the negative anomaly of specific humidity is found to have been developed more northward of the convection centre than in the observation. The moist static energy also shows coherence with the observation except that after 96 h lead time, the southward tilt is not captured and that the region of instability is found to be more north of the convection centre than in the observation data (Fig. 28a–d). Moreover, moisture convergence also follows the above characteristic (Fig. 29a–d). There is a decrease in the depth of the layer where convergence is occurring. At 24 h lead time, moisture convergence could be seen until 700 hPa but at 96 h lead time, it drops down to 850 hPa. In case of break phase, vorticity is captured quite well throughout all the lead times (Fig. 30a–d). A decrease in magnitude is seen after 96 h forecast lead time.

A low tropospheric temperature is also an indicator of break phase of monsoon. The tropospheric temperature is still higher for higher latitudes but as can be clearly seen from Fig. 31, the gradient has considerably reduced as compared to the active period which results in weakening of the monsoon circulation and hence the break phase of monsoon is seen. The wind shear profile also shows a weakening in Fig. 32 in terms of both magnitude and slope indicating the weakening of tropical easterly jet. Again, following Jiang et al. 2004, a decreased easterly shear causes a decrease in strength of the barotropic vorticity, which leads to suppressed moisture convergence. Hence, this contributes to the decreased rainfall in the break period.
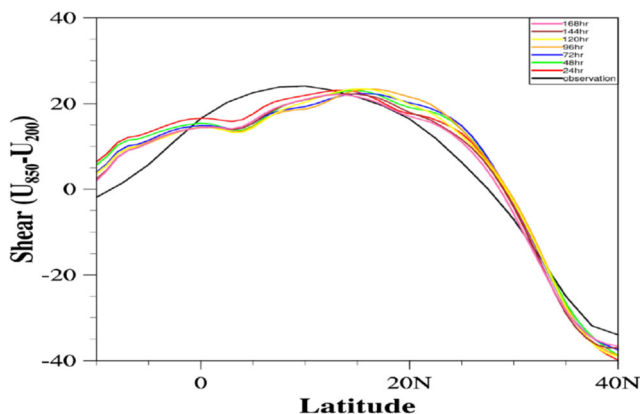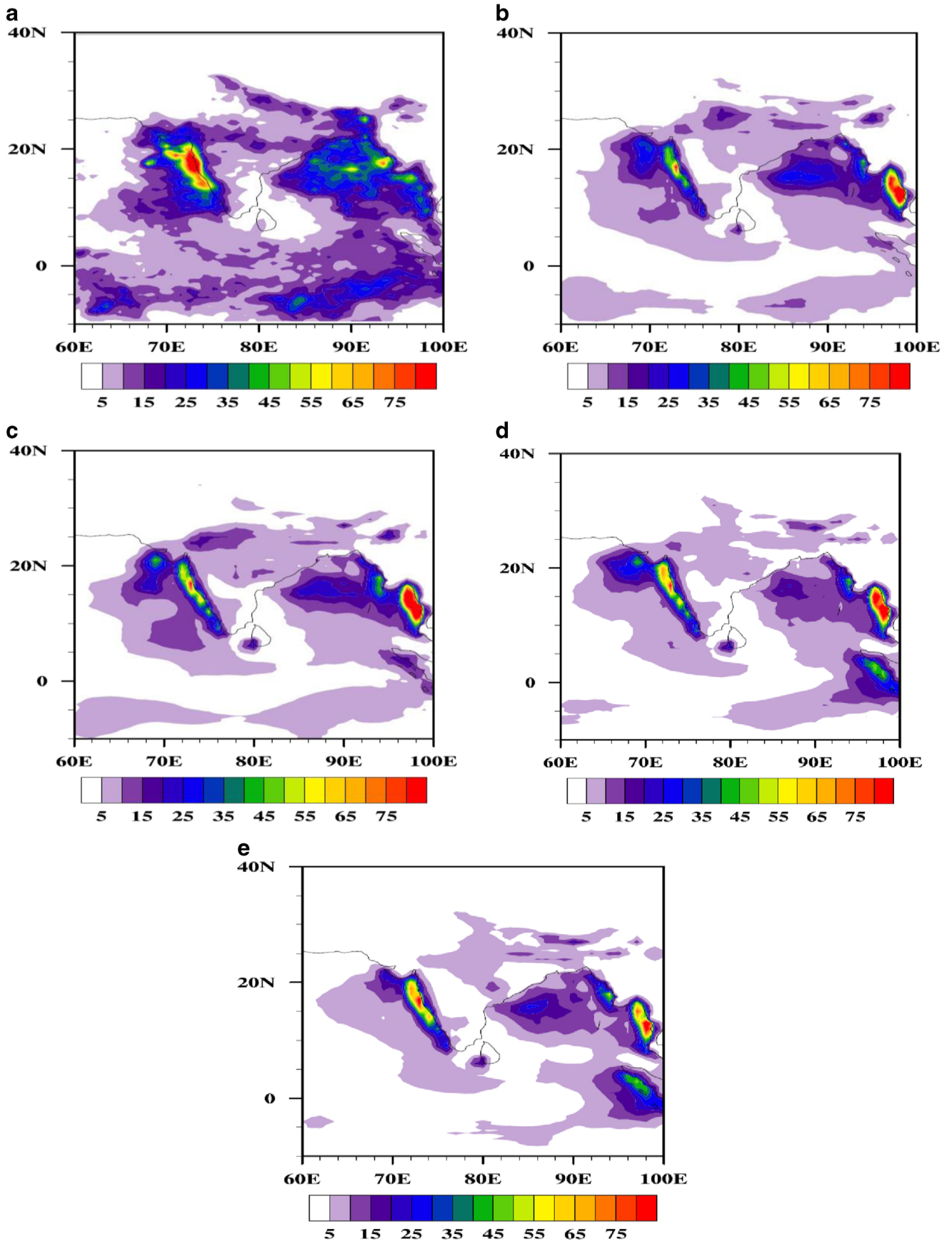

Fig. 32 Wind shear for the active period meridionally averaged over 70°E–90°E using NCEP/NCAR Reanalysis data for the period 2006–2011

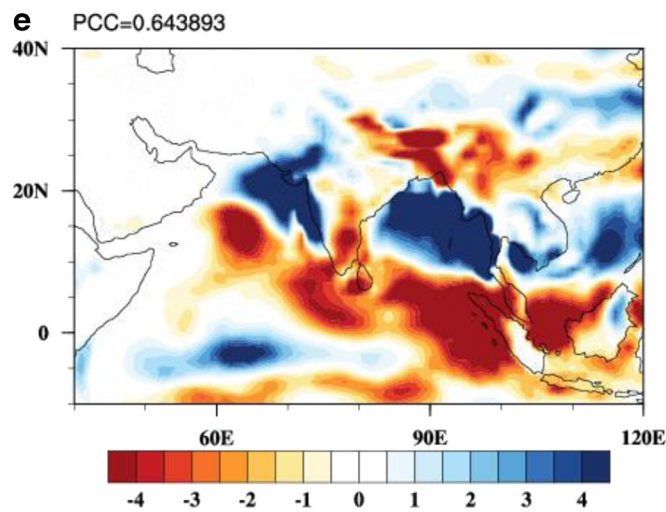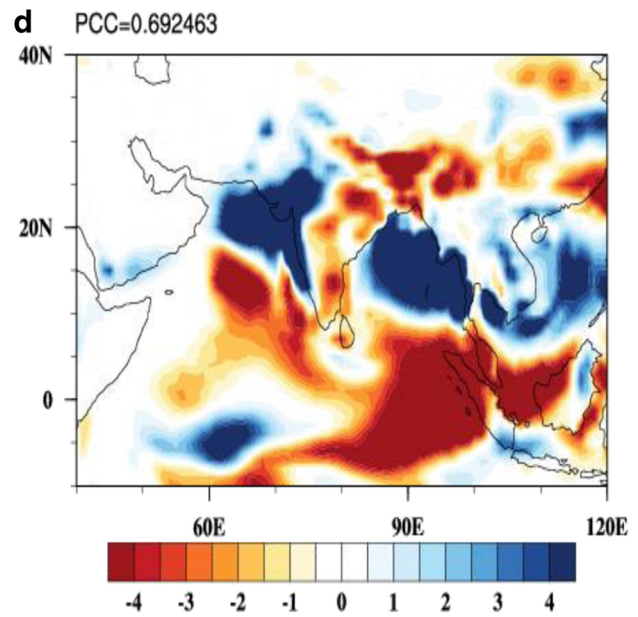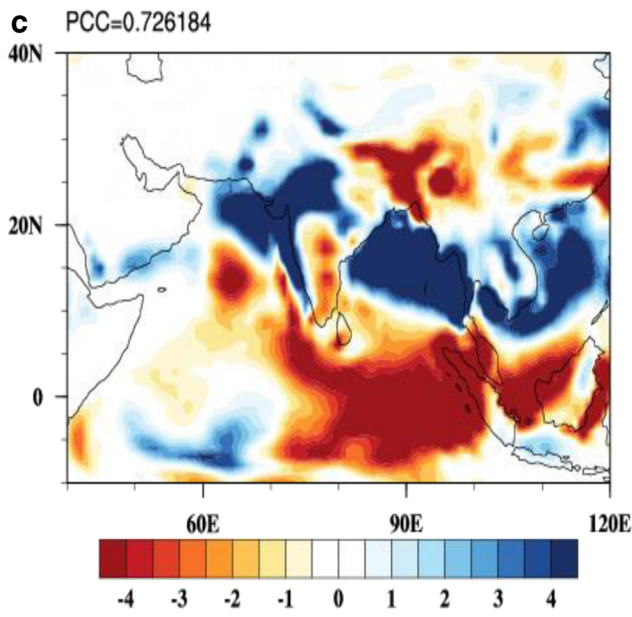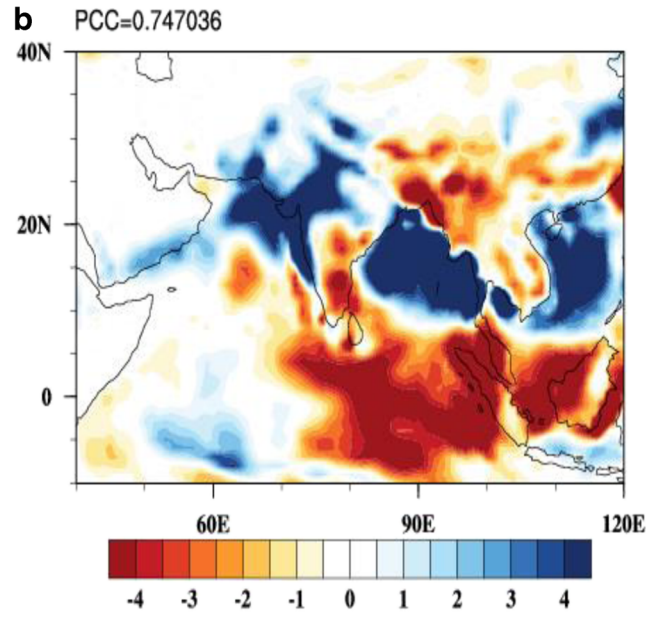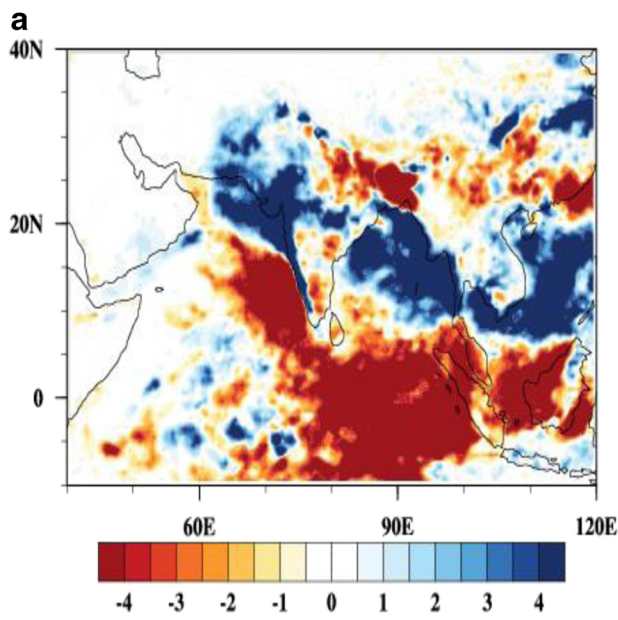Fig. 33 Intraseasonal variability of JJAS rainfall for **a** TRMM 3B42 ▶ precipitation (mm^{-2} day^{-2}), **b** 24 h, **c** 48 h, **d** 96 h, **e** 168 h NCEP EPS forecast precipitation (kg^{-2} m^{-4})

◀ **Fig. 34** Composite of rainfall for active days of good monsoon years for (**a**) TRMM 3B42 precipitation (mm day^{-1}), (**b**) 24 h, (**c**) 48 h, (**d**) 96 h, (**e**) 168 h NCEP EPS Forecast precipitation (kg m^{-2})

To further ponder on this notion, variance calculated at each grid point from the NCEP EPS precipitation data shows a diminished picture when compared to observations. With increasing lead times, the variance shows considerable decrease as is evident from Fig. 33.

3.3 Analysis of good and deficient monsoon years

The performance of NCEP EPS during good and deficient monsoon year is analysed. The composite of active days for good monsoon year (Fig. 34) clearly shows that the forecast captures the spatial characteristics of precipitation anomaly very well with pattern correlation coefficient of 0.75 for 24 h lead time and decreasing to 0.64 for 168 h lead time. Also, the composite of break days for deficient monsoon year (Fig. 35) shows that the forecast reasonably performs in case of deficient year too with pattern correlation coefficient of 0.75 for 24 h lead time to 0.66 for 168 h lead time. Even the break days of good monsoon year and active days of deficient monsoon year show spatial resemblance to the observation with pattern correlation coefficient decreasing with lead time from 0.75 to 0.66 and 0.63 to 0.41 for 24 to 168 h respectively (figures not shown).

To further account for the skill of forecast, Fig. 36 shows the anomaly correlation coefficient. The correlation decreases with increasing lead time. The JJAS months for deficient monsoon year (green) show very good correlation even up to 7-day lead time. This might be due to the fact that the atmosphere lacks organized convection and dominant northward propagation (Abhik et al. 2013) during such a period and hence possibly the model could capture the environment with better fidelity. On the other hand, correlation of above 0.5 is seen for JJAS of good monsoon year (blue) up to 2-day lead time. Also when calculating the correlation for only active (orange) and break (purple) days, the values are lower than for the season (red), with the break days showing better correlation than active days. It decreases with lead time generally but shows a slight increase at 4–5-day lead time. This gives an indication that the EPS is able to predict the mean state of the season with some fidelity, but it still finds it challenging in capturing the active days with sufficient lead time.

4 Conclusions

Predictability of MISO has always been a challenging task. Our present study is an attempt to analyse the MISO with NCEP EPS daily forecast data. There have been studies to analyse MISO with EPS data but not on daily time scale. It is observed that the spatial characteristics and northward propagation of MISO are well captured by the EPS up to 168 h (7 days) forecast lead time. The pattern correlation shows that the forecast agrees well with the observation up to forecast lead time of 96 h for all lags. When the genesis and propagation of the convection belt are analysed, we find that the development of anomalous specific humidity starts growing from lower troposphere and gradually go towards middle troposphere. The anomaly also exhibits a southward tilted structure which is a characteristic feature of monsoon convection as per Jiang et al. 2011; Abhik et al. 2013. The evolution of moist static energy in the EPS data is also seen to adhere to the observation up to 96 h lead time. Also, the pattern of moisture convergence agrees to the observation until 96 h lead time but tumbles for lead times beyond 96 h. Thus, the instability associated with precipitation is captured well by the EPS data for lead time up to 96 h. The tropospheric temperature that drives and maintains the monsoonal circulation also shows adherence to the observation albeit with a bias in magnitude. The wind shear pattern is also very well simulated by the forecast throughout the increasing lead times. Thus, we can say that the requirements necessary for northward propagating MISOs is well captured by the EPS up to 96 h. However, accuracy in forecast with longer lead times with regard to its thermodynamics and physics could not be produced. Coming to the skill of the model, the anomaly correlation is comparatively better for the whole season than individual active days indicating towards the fact that the average picture is better simulated than particular events or weather. This is further fortified when we observe the variance throughout the lead times and the observations. The predicted variance is found to be well captured by the model up to a lead time of 96 h. However, it weakens with increasing lead time. The composites of precipitation anomaly for the active and break events of good and deficient monsoon years show that the EPS performs fairly well in case of good and deficient years with anomaly correlation coefficient of deficient monsoon year being higher than good monsoon year.

We can deduce from the above discussion that the spatial characteristics of MISO are very well captured by the EPS in the short range. The analysis of thermodynamical and dynamical parameters shows that for
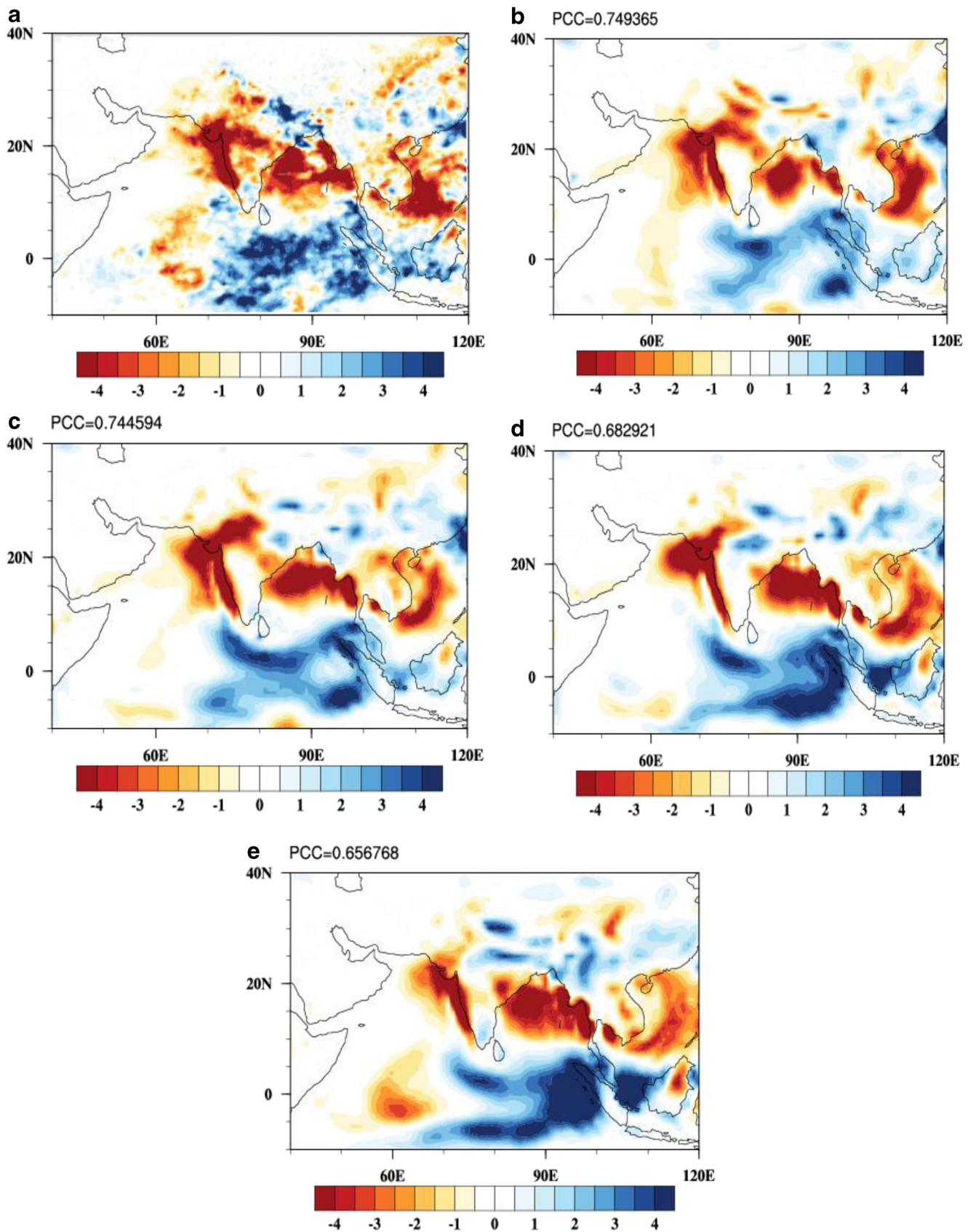
Fig. 35 Composite of rainfall for break days of deficient monsoon years for **a** TRMM 3B42 precipitation (mm day^{-1}), **b** 24 h, **c** 48 h, **d** 96 h, **e** 168 h NCEP EPS forecast precipitation (kg m^{-2})
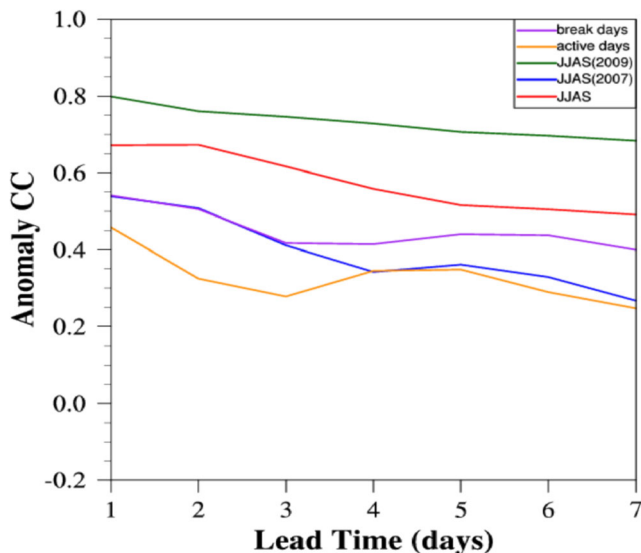
Fig. 36 Anomaly correlation coefficient for rainfall with respect to lead time and area averaged over Central India (18°N–25°N, 73°E–85°E) using TRMM 3B42 for observation and NCEP TIGGE EPS for forecast

shorter lead times the forecast very well matches the observations. It incorporates moisture, U and V components of wind fairly well. But as the lead time increases, the error in forecast of these parameters also increases, resulting in the inaccuracy in forecasted rainfall. Hence, we can say that the incorporation of better assimilation of moisture in the model will lead to a better forecast of precipitation. The EPS also shows considerable effectiveness in maintaining the integrity of forecast when assessed particularly for excess and deficient years. Use of probabilistic approach for forecasting is undeniable, but we also have to keep in mind the improvement of model physics. This will develop the basis for attempting such EPS technique for Indian monsoon application. Our study shows that MISO is very well captured in EPS in the short range. Hence, the ensemble approach should be incorporated in CFS/GFS system to quantify the uncertainties. Also, sensitivity tests with various schemes for model physics can be undertaken to find out the best possible combination of convection, radiation schemes etc. that compliments the Ensemble Prediction System.

References

Abhik S, Halder M, Mukhopadhyay P, et al. (2013) A possible new mechanism for northward propagation of boreal summer intraseasonal oscillations based on TRMM and MERRA reanalysis. Clim Dyn 40:1611–1624. doi:10.1007/s00382-012-1425-x

Abhilash S, AK S, Borah N, et al. (2014) Prediction and monitoring of monsoon intraseasonal oscillations over Indian monsoon region in an ensemble prediction system using CFSv2. Clim Dyn. doi:10.1007/s00382-013-2045-9

Chen S-C, JO R, JC A (1992) Variability and predictability in an empirically forced global model. J Atmos Sci 50:443–463

Chen T-C, Alpert JC (1990) Systematic errors in the annual and intraseasonal variations of the planetary-scale divergent circulation in NMC medium-range forecasts. Mon Weather Rev 118:2607–2623

Duchon CE (1979) Lanczos filtering in one and two dimensions. J Appl Meteorol 18:1016–1023

Gadgil S (2003) The Indian monsoon and its variability. Annu Rev Earth Planet Sci 31:429–467. doi:10.1146/annurev.earth.31.100901.141251

Gadgil S, Gadgil S (2006) The Indian monsoon. GDP and Agriculture: 4887–4895

Goswami BB, Mani NJ, Mukhopadhyay P, et al. (2011) Monsoon intraseasonal oscillations as simulated by the superparameterized Community Atmosphere Model. J Geophys Res Atmos 116:n/a–n/a. doi:10.1029/2011JD015948

Goswami BN (2005) South Asian monsoon, chapter 2. In: WKM L, DE W (eds) Intraseasonal variability of the atmosphere ocean climate system, pp. 19–61

Goswami BN, Wu G, Yasunari T (2006) The annual cycle, intraseasonal oscillations, and roadblock to seasonal predictability of the Asian summer monsoon. J Clim 19:5078–5099

Goswami BN, Xavier PK (2005) ENSO control on the south Asian monsoon through the length of the rainy season. Geophys Res Lett 32: L18717. doi:10.1029/2005GL023216

Huffman GJ, Bolvin DT, Nelkin EJ, et al. (2007) The TRMM multisatellite precipitation analysis (TMPA): quasi-global, multiyear, combined-sensor precipitation estimates at fine Scales. J Hydrometeorol 8:38–55. doi:10.1175/JHM560.1

Jiang X, Li T, Wang B (2004) Structures and mechanisms of the northward propagating boreal summer intraseasonal oscillation *. J Clim 17:1022–1039

Jiang X, Waliser DE, Woods C (2011) Vertical cloud structures of the boreal summer intraseasonal variability based on CloudSat observations and ERA-interim reanalysis. Clim Dyn. doi:10.1007/s00382-010-0853-8

Kalnay E, Kanamitsu M, Kistler R, et al. (1996) The NCEP/NCAR 40-Year Reanalysis Project, vol 77, pp. 437–471

Krishnamurti TN, Subramanyam D (1982) The 30–50 day mode at 850mb during MONEX. J Atmos Sci 38(9):2088–2095

Liess S, Waliser DE, Schubert SD (2005) Predictability studies of the intraseasonal oscillation with the ECHAM5 GCM. J Atmos Sci 62:3320–3336

Lorenz EN (1963) Deterministic nonperiodic flow. J Atmos Sci 20:130–141

Pattanaik DR, Kumar A (2009) Prediction of summer monsoon rainfall over India using the NCEP climate forecast system. Clim Dyn 34: 557–572. doi:10.1007/s00382-009-0648-y

Reichler T, Roads J-O (2005) Long-range predictability in the tropics. Part II : 30–60-day variability. J Clim 18:634–650

Sahai AK, Sharmila S, Abhilash S, et al. (2013) Simulation and extended range prediction of monsoon intraseasonal oscillations in NCEP CFS/GFS version 2 framework. Curr Sci 104: 1394–1048

Sikka DR, Gadgil S (1980) On the maximum cloud zone and the ITCZ over Indian longitudes during the southwest monsoon. Mon Weather Rev 108:1840–1853

Suhas E, Neena JM, Goswami BN (2012) An Indian monsoon intraseasonal oscillations (MISO) index for real time monitoring and forecast verification. Clim Dyn 40:2605–2616. doi:10.1007/s00382-012-1462-5

Taraphdar S, Mukhopadhyay P, Goswami BN (2010) Predictability of Indian summer monsoon weather during active and break phases using a high resolution regional model. Geophys Res Lett 37:n/a–n/a. doi:10.1029/2010GL044969

Waliser D (2012) Predictability and forecasting. In: Lau WKM, Waliser DE (eds) Intraseasonal Var. Atmos. Clim. Syst., second edn. Springer-Praxis, pp 433–476

Waliser DE, Stern W, Schubert S, Lau KM (2003) Dynamic predictability of intraseasonal variability associated with the Asian summer monsoon a) India b) S E Asia. Q J R Meteorol Soc 129:2897–2925. doi:10.1256/qj.02.51

Webster PJ, Magana VO, Palmer TN, et al. (1998) Monsoons : processes, predictability, and the prospects for prediction 2. Description of the monsoons. J Geophys Res 103:14451–144510

Yang S, Zhang Z, Kousky VE, et al. (2008) Simulations and seasonal prediction of the Asian summer monsoon in the NCEP climate forecast system. J Clim 21:3755–3775. doi:10.1175/2008JCLI1961.1

Yasunari T (1979) Cloudiness fluctuations associated with the Northern Hemisphere Summer Monsoon. J Meteorol Soc Japan:227–242

Yasunari T (1981) Structure of an Indian summer monsoon system with around 40-day period. J Meteorol Soc Japan:336–354